# Some Studies on Design and Simulation of Microstrip Slot Loaded Miniaturized Patch Antenna Based Smart Tracking System using Beam Steering Technique

By
**Paramita Saha**
Registration No: 150142 of 2019-2020
Class Roll No.: 001910703015
Exam Roll No. M6VLS22014

Under the Guidance of:
**Prof. P. VENKATESWARAN**

Thesis submitted in partial fulfillment of the requirements
for the award of the Degree of Master of Technology in
VLSI Design and Microelectronics Technology

Department of Electronics and Telecommunication Engineering
Jadavpur University
Kolkata- 700032

August 2022

# DECLARATION OF ORIGNALITY AND COMPLIANCE OF ACADEMIC ETHICS

I hereby declare that this Thesis contains literature survey and original work by the undersigned candidate, as part of her Master of Technology in VLSI Design and Microelectronics Technology.

All information in this document have been obtained and presented in accordance with academic rules and ethical conduct.

I also declare that, as required by these rules and conduct, I have fully cited and referenced all material and results that are not original to this work.

Name of the Candidate: **Paramita Saha**

**Exam Roll No.: M6VLS22014**

Thesis Title: **Some Studies on Design and Simulation of Microstrip Slot Loaded Miniaturized Patch Antenna Based Smart Tracking System using Beam Steering Technique.**

**Signature of the Candidate: ----------**

**Date:**

# FACULTY OF ENGINEERING AND TECHNOLOGY

# JADAVPUR UNIVERSITY

## CERTIFICATE OF RECOMMENDATION

I hereby recommend that this Thesis prepared by Paramita Saha entitled **Some Studies on Design and Simulation of Microstrip Slot Loaded Miniaturized Patch Antenna Based Smart Tracking System using Beam Steering Technique** under my supervision be accepted for partial fulfillment of the requirements for the award of the Degree Master of Technology in VLSI Design and Microelectronics Technology

……..

**Dr. P. Venkateswaran**

Professor

Dept. of Electronics and Tele-Communication Engineering

Jadavpur University, Kolkata- 700032

……

**Dr. Manotosh Biswas**

Professor and Head

Department of Electronics and

Telecommunication Engineering,

Jadavpur University, Kolkata- 700032

.....……..

**Prof. Chandan Mazumdar**

Dean

Faculty of Engineering and Technology

Jadavpur University, Kolkata- 700032

# FACULTY OF ENGINEERING AND TECHNOLOGY

# JADAVPUR UNIVERSITY

## CERTIFICATE OF APPROVAL*

The foregoing Thesis is hereby approved as a creditable study of an engineering subject carried out and presented in a manner satisfactory to warrant its acceptance as a prerequisite to the Degree for which it has been submitted. It is understand that by this approval, the undersigned don't necessarily endorse or approve any statement made, opinion expressed or conclusion drawn therein but approve the Thesis only for the purpose for which it is submitted.

Committee on ……

Final examination for

Evaluation of the thesis of:

**PARAMITA SAHA**

Exam Roll No: M4ETC19014 ……

……

Signature of Examiners

* Only in case the thesis is approved.

# ACKNOWLEDGEMENT

I express my deep sense of gratitude and indebtedness to my Thesis Supervisor, Prof. Palaniandavar Venkateswaran, Department of Electronics & Tele-Communication Engineering, Jadavpur University, Kolkata, for providing me the opportunity to carry out the Thesis work. I am grateful to him for his parental guidance, valuable insights and suggestions that he gave me throughout my M. Tech Thesis work.

Further, I express my special thanks to Mr. Jagabandhu Das, Department of Millimeter Integrated Chip Fabrication SAMEER, Kolkata, for his excellent technical assistance and guidance.

I would also like to thank Prof. Subir Kumar Sarkar, Dr Manotosh Biswas, Head, Department of Electronics & Tele- Communication Engineering, Jadavpur University for their compassionate approach. I would like to express my sincere gratitude to all the teaching and non-teaching staffs of the department for providing necessary support.

Last but not the least, this work would not have been possible without the love, support and encouragement of my husband Mr. Aritra Roy, my parents, my parents in law, classmates and near and dear ones.

Computer Networking Lab (T-3-16A)

ETCE Dept., Jadavpur University

Kolkata - 700 032. West Bengal.

August 2022

**……..……..**

**PARAMITA SAHA**

# SYNOPSIS

In this Thesis work, a beam steering technique based smart tracking system is investigated to maximize the utilization of the radiated power from a base station towards a mobile user. The tracking operation is performed in the receiving chain that uses a received magnitude-based analysis to determine the user location accurately. The working principle of this technique is investigated numerically by moving a dipole (user) in front of a $1 \times 2$ patch antenna array in the longitudinal and lateral directions, and the relation between the received magnitude levels with relative user location is established. The magnitude comparison is performed in the DC domain instead of RF to simplify this operation by avoiding the RF processing circuits. The RF outputs of each antenna are converted into DC using a rectenna circuit which consists of a single diode having a conversion efficiency of $42\%$. Since the DC voltages can have an analog variation in their amplitude, an op-amp based comparator circuits is designed to convert these voltages into digital levels. They are further processed using a Boolean Logic Circuit to index the antenna element receiving the maximum RF from the user. As the antenna closest to the user has the minimum Euclidean distance between them, it will receive the maximum RF power from the moving user. Hence, the user location relative to the antenna array can be accurately determined with the above-mentioned antenna index. Once, the user location is determined, the antenna beam is steered at that direction. The steering is performed in the transmitting chain that uses the conventional phased array technique. It simplifies the steering circuit over other reported techniques in the literature, and can provide a good angular accuracy. The antenna index in the receiving chain is used to generate the required phase value to tilt the overall radiation towards user. A simple passive and lossless power divider and phase shifter circuit are designed and investigated with the proposed antenna array. Both the receiving and transmitting chains use a single antenna array for tracking and steering operations, respectively. The array is designed using an asymmetrically placed slot loaded miniaturized patch antenna to operate at $2.45GHz$. The beam steering operation is also carried out with the proposed antenna array in conjunction with the phase shifter circuit where the beam is steered over an angle of $\pm 22^0$ in the azimuthal direction. The transmit and receive chains are connected to the antenna using a circulator that works as a decoupling network and isolates the two sections by maintaining a unidirectional flow of EM power in the transceiver chain. A conventional ferrite loaded circulator as well as ferrite less circulator are designed and investigated here. The ferrite circulator has good impedance matching, with insertion loss of $-1.8dB$ and more than -

$30dB$. isolation. Since, the presence of ferrite makes the circuit non-planar, a ferrite less approach is also investigated to design a planar circulator. Two Branch line couplers and one asymmetric Wilkinson power divider is used to design ferrite less circulator. Though the design is having a reduced isolation, it exhibits higher insertion loss, and provided here as a new design concept.

# CONTENTS

# List of Figures

# List of Tables

# CHAPTER 1

# Introduction

## 1.1. Preamble

Antenna beam scanning and Beam steering techniques have been widely used over decades to communicate with a user by utilizing the maximum radiation of the antenna. The user location is identified using different detection techniques which are followed by the movement of the antenna main beam at that direction. These techniques were developed especially for radar applications for electronic warfare to detect the presence of a target far away. It is an effective approach to communicate with a user with the full capacity of an antenna radiation by guiding the antenna main beam at that direction after detecting the location of user which using the scanning technique. Followed by its success in radar applications, the scanning and beam steering techniques are adopted simultaneously for different domestic applications including the modern day high-speed, multiuser cellular technology. In these applications, the user locations under certain base stations are identified by scanning and then antenna main beam is steered towards the user using different beam steering techniques.

Different types of scanning techniques were investigated to detect a user location correctly. In radar tracking system using single track scattering, a single user is tracked with a high data rate for an accurate tracking of its location. Monopulse radar [1] is a typical single tracking system which is used widely to track a moving target effectively [2,3]. This technique is also useful to launch counter attack during the war especially with those using missiles. This approach is accurate but requires a wide bandwidth with multiple receiving channels at high data rate with multiple antennas being used. A single receiving channel or a single antenna is used in a typical conical scan approach [4], where the conical movement of the antenna main beam is combined with the received signals to detect the user location. This approach is less accurate than the previous one but can work with a simple and cost effective system chain. A mechanical scanning system [5] utilizes a single antenna with a narrow beam to detect several users over the wide area by rotating the antenna main beam mechanically. This process is cheap and cost effective and may be suitable for commercial air-surveillance systems. An automatic track and detection system [6] uses a similar scanning technique to detect and track the users using software based detection systems. This process is slow but simple and can track a large number of users simultaneously with good accuracy. A track while scan system [7, 8] is another sub class of an automatic tracking system, where the beam is moved over a limited angular location to detect a modest number of users simultaneously with a better accuracy. This can be implemented by two scanning fanbeams in perpendicular arrangement or by four monopulse beam scanning antennas for scanning in azimuth as well as in elevation. A phased array tracking system [9,10] is a smart scanning technique to detect multiple objects at a faster rate by switching antenna main beam electronically. The electronic switching of antenna main beam is implemented by changing the phase of antenna inputs of an antenna array. The scanning or tracking systems [11] can also be classified based on the movement of the antenna main beam in the spatial domain. Circular scan, helical scan, raster scan, sector scan, conical scan etc., are employed for different applications based on the design requirements such as accuracy, speed, power, bandwidth, fabrication cost etc.

The scanning system is followed by the beam-steering or beam-forming [13,14] stage where the antenna main beam is guided at the user location. Mechanical steering [15] is one of the oldest techniques used for this purpose which is slow and inaccurate and generally bulky in size. On the contrary, a beam forming network using phased array approach [16,17] is fast and accurate but requires additional circuit complexity and extensive background computation. A reflect-array or transmit-array configuration [18] uses a single aperture antenna whose radiated field are guided at different directions by reflecting the transmitted

radiated waves using engineered surface. The surfaces have phase gradient along the structure [19] which can be suitably tailored to guide the antenna main beam at different directions. These approaches are having severe challenges during their design phase, but simple and cost effective. Similar functionality can also be achieved by placing a parasitic layer consisting of a set of metallic patches of different shape and size near the antenna. It is simple in design but can affect the input impedance of the antenna significantly. Moreover, the steering of main beam may not be accurate, and the beam width may change for different configurations of the parasitic surface. Integrated lens antenna [20,21] works on the similar working principle as the previous approaches but having the similar limitations. Multiple antennas can be placed towards different angular location forming a non-planer array of the radiators. This approach does not possess the smooth and linear change in the steering angle having fixed apertures at fixed directions. A leaky wave antenna is a non-resonant traveling wave antenna having a steered beam over a wide angle [22]. But the steering angle varies with frequency facilitating the same in only one dimension. Metamaterial based beam steering approaches [23] are also reported in literature where the control on the main beam is difficult and the antenna performances can be severely affected.

## 1.2. Motivation

In this Thesis work, design of a base station transceiver system is carried out by designing the scanning/tracking [7-11] system followed by the beam steering [24-27] of an antenna array. Movement of the antenna main beam is restricted over azimuthal direction hence a one dimensional beam scanning and steering approach is investigated. From the available literature, it is understood that a phased array system can have a better control on the direction of antenna main beam which can even match with the analytical predictions. For scanning, both amplitude and phase information are used in most cases that delays the background process with a complex system. Moreover, most of the processing happens in the RF domain i.e., the RF signals are directly processed to make a decision about the user location. The RF signal processing circuits are complicated and require additional expertise to design the corresponding RF circuit. It increases the cost and complexity of the detection network. Also, a compact circuit including the antenna is to be designed to make the overall transceiver design compact. Hence, a compact scanning-beam steering technique is to be implemented using a simple and cheap architecture with an accurate control for a reliable design of transceiver.

## 1.3. Literature Survey

The idea behind the beam scanning [7-11] and beam steering [24-30] was discussed in the previous section. Antenna being an indispensable component of this circuit provides a wide range of flexibility in its design [31]. Miniaturization of antennas is one of the most important topics for modern day antenna designers. Different techniques have been reported to make the antenna small [32] such as with dielectrics [33], with slots [34] or even with metamaterials [35]. The slot based technique is one of the compact and easiest approaches in which no additional elements are appended to the primary radiator. It offers capacitive effect and elongates the current path to miniaturize the antenna element effectively. A power divider circuit is one that divides the incoming power among multiple paths. Different types of standard power division circuits are available in the literature such as

- Wilkinson Power Divider [36,37]
- Branch-line coupler [38-41]
- Rat-race coupler [42-45] etc.

To investigate the beam steering operation, a phase shifter circuit is needed to design with the power divider circuit. Depending upon the geometry, there are different types of RF phase shifters as follows:

- Switched line phase shifter [46-49],
- Hybrid coupled line phase shifter [50-53] and
- Periodically loaded line phase shifter [54,55].

In this Thesis work, a corporate fed combined power divider phase shifter [57-59] circuit is designed as it offers less design complexity. To provide isolation between transmitting and receiving chain of the any tracking or scanning system in wireless communication, a coupling-decoupling circuit is needed. Circulator [60-67] is a typical three or four port network used in RF system that offers a perfect isolation between transmitting and receiving section. Circulators are basically two types:

- Ferrite circulator and
- Non-ferrite circulator.

A ferrite circulator is the most common commercially available geometry that uses a ferrite material for non-reciprocity. Its design is simple and compact except the ferrite has to

be suitably placed in the three-port network. Non-ferrite based circulators have shown significant promise that can avoid the ferrite easily. It generally consists of multiple coupler and power dividers to achieve the isolation between the desired ports. The geometries are generally bulky and the isolation is not as good as a ferrite one.

Rectenna [68-72] is a circuit that is used to convert RF power to usable DC electrical energy. Several research papers introduced the single band simple structured rectenna as well as multiband complex structure rectennas. These are widely used for applications like energy harvesting and wireless power transfer.

## 1.4. Research objective

In this Thesis, a new scanning and beam steering technique is designed to implement a transceiver system in a mobile base station.

- To scan/track the user location,
    - A rectenna circuit is designed to convert the RF signals into equivalent DC levels.
    - A DC level comparator circuit is proposed to determine the user location correctly. The decision making circuit consists of simple DC magnitude comparators unlike the complex RF comparators in the available literature / existing design.
- To steer the antenna main beam towards the user
    - A power divider and phase shifter circuit is designed to observe the steering capability of the proposed antenna array.
- To transmit and receive the Electron Magnetic (EM) signal,
    - A slot loaded miniaturized patch antenna is designed along with its array.
    - A coupling-decoupling system is developed to maintain the unidirectional flow of EM signals between the transmit-receive system and antenna.

All the design / investigations are carried out numerically using CST Studio Suite and Keysight ADS EM simulators.

## 1.5. Thesis Organization

The Chapters of the Thesis are organized as follows:

**In Chapter 1**, the literature review is presented citing appropriate published articles. The review is done in diverse direction as different circuit components and systems are addressed in this thesis. Literatures on conventional antennas, array of antennas, antenna beam scanning, power divider, phase shifter and circulator circuits and rectenna have been reviewed in this chapter.

**In Chapter 2**, the design of the proposed patch antenna with 1x8 array of the antenna patch numerical outputs is presented. The design of a power divider and phase shifter circuit is also presented. Both items are designed individually and are assembled for the desired outcome. This circuit is used to validate the beam forming and beam steering by the patch array by varying the phases of individual antenna elements.

**In Chapter 3**, design of a conventional diode based rectenna circuit and a digital logic circuit is presented. The rectenna will be used to convert the received RF signals into DC which will be used to determine the relative position of the user about the antenna array. The outputs are analysed both in frequency domain, and time domain to determine the effectiveness of the circuit. The digital logic circuit is designed using op-amp and basic gates to determine the maximum power received by rectenna. The objective of the DC circuit is to produce an output to determine the antenna location receiving the maximum RF.

**In Chapter 4**, the working of the overall transmitting and receiving RF chain of the proposed smart tracking system is discussed with block diagrams. Design of a circulator circuit is also presented here that can work as the decoupling network between the transmitting and receiving RF chain at the antenna. The variation of received power with the relative location of the user about the antenna array is investigated numerically. A dipole antenna is designed and is moved near an array to observe the difference in power at each antenna output. At the end of this chapter, a schematic of the proposed system in total is described.

**In Chapter 5**, the conclusion and future works are presented.

# CHAPTER 2

# Proposed Beam Steering Technique using Slot Loaded Miniaturized Microstrip Patch Antenna

## 2.1. Introduction

Microstrip patch antenna is an essential radiator widely used for commercial communication systems. To design a compact system, the antenna geometry is to be miniaturized preserving its primary radiation properties. In this chapter, a miniaturized slot loaded patch antenna is designed and an antenna array is investigated to facilitate a beam steering mechanism. A simple phased array antenna can serve the purpose of beam steering accurately by controlling the phase of the input antenna signals. A similar phase shifter circuit is also investigated to understand the steering mechanism of the proposed antenna. A corporate feed power division circuit is also designed to feed the antennas using a single RF source as is done in most microwave systems.

## 2.2. Design of Proposed Antenna and Antenna Array

### 2.2.1. Proposed Slot Loaded Miniaturized Microstrip Patch Antenna

**Schematic**

The reference antenna is a rectangular patch antenna designed to work at a higher frequency. Schematic of the antenna is similar to that in Fig.2.1 without the slot. The patch has a length of $l_p = 13.9$ mm and a width of $w_p = 18.4$ mm. It is printed on a FR-4($\epsilon_r = 4.3$), ($\tan\delta = 0.025$) substrate of thickness 1.6 mm of length $l_{sub} = 50$mm and $w_{\text{sub}} = 50$mm. The patch is exited with a coaxial line placed 3 mm below the antenna centre.

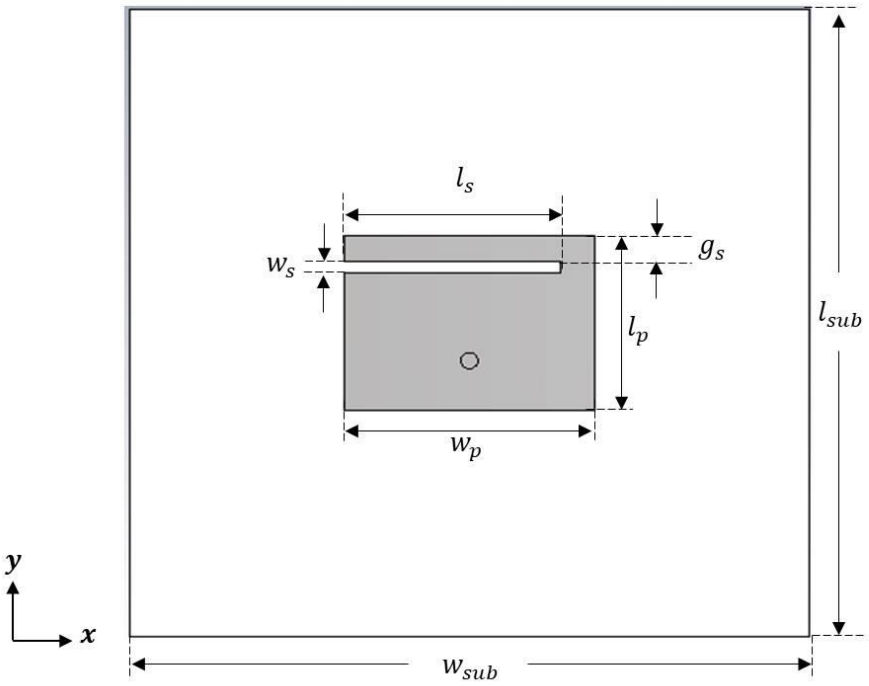


Fig. 2.1: Schematic of the proposed antenna

The dimensions of the rectangular microstrip patch are calculated by using the following equations. Equations given below are used for the calculation of the perimeter of the rectangular patch in terms of length ($L$) and width ($W$),

$$W = \frac{c}{2f_0\sqrt{\frac{(\epsilon_r+1)}{2}}} \tag{2.1}$$

$$\epsilon_{e_{ff}} = \frac{\epsilon_r+1}{2} + \frac{\epsilon_r-1}{2}\left[1 + 12\frac{h}{W}\right]^{\frac{1}{2}} \tag{2.2}$$

$$L_{eff} = \frac{c}{2f_0\sqrt{\epsilon_{eff}}} \tag{2.3}$$

$$\Delta L = 0.412h\frac{(e_{ff}+0.3)\left(\frac{W}{h}+0.264\right)}{(e_{ff}-0.258)\left(\frac{W}{h}+0.8\right)} \tag{2.4}$$

$$L = L_{eff} - 2\Delta L \tag{2.5}$$

Where, $\epsilon_{eff}$ = Effective dielectric constant of the patch

$L_{eff}$ = Effective length of the patch

The simulated $S_{11}$ of the reference antenna is shown in Fig.2.2. The antenna resonates around $5GHz$ (4.84~GHz) as the $S_{11} < -10dB$ at this frequency. The antenna dimensions are determined using [4], for a frequency approximately double of our frequency of interest ($2.45GHz$, centre of the ISM band). To reduce the operating frequency of this antenna, a horizontal slot is placed asymmetrically as shown in Fig.2.1. The slot has a length of $l_s$ and width of $w_s$ maintains a gap of $g_s$ from the top edge. This slot significantly miniaturizes the antenna and the overall performance can suitably be tuned by varying its dimensions as is discussed in the following sections.

**Effects of Slot Length ($l_s$)**

Simulated responses by varying the slot length ($l_s$) are summarized in Fig.2.2. Both slot width ($w_s$) and slot gap ($g_s$) are fixed at 1 mm in this investigation. It can be observed that by increasing $l_s$, the resonant frequency can be significantly being shifted down to lower frequencies. For example, by varying the length from $5\,mm$ to $15\,mm$, the resonance is shifted from $4.66\,GHz$ to $2.56GHz$ which is approximately half of that of the reference antenna. The antenna is resonated at $2.45GHz$ with $l_s$ = $15.9\,mm$. The slot elongates the current path on antenna and reduces the resonant frequency with an increased slot length.

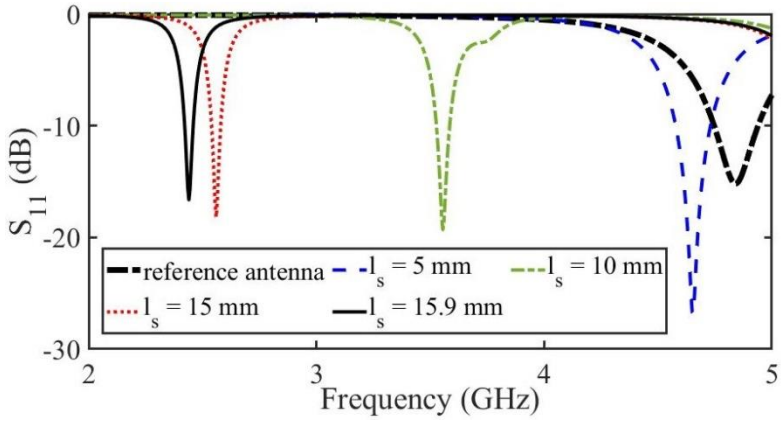


Fig. 2.2: Simulated $S_{11}$ of the reference antenna with varying slot length $l_s$

**Effects of Slot Width ($w_s$)**

In this investigation, the slot width is varied by keeping $l_s = 15.9\,mm$ and $g_s = 1\,mm$. The simulated responses are summarized in Fig.2.3. It is observed that, the resonant frequency shifts down by increasing the slot width. A higher $w_s$ increases the slot perimeter, thereby reduces the operating frequency of it. But, a degraded impedance matching is observed with the increment in slot width. With a wider slot, the current distribution on antenna is disturbed and the impedance at the feed point is deviated from 50 Ω. Hence, a poor matching is observed with a wider slot. The $S_{11} < -10\,dB$ is observed at $2.45GHz$ with $w_s = 1\,mm$.

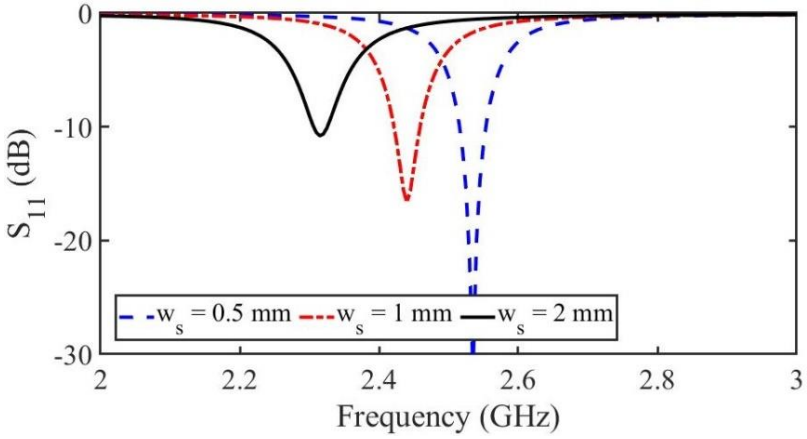


Fig. 2.3: Simulated $S_{11}$ with varying slot width $w_s$

**Effects of slot gap ($g_s$)**

The simulated $S_{11}$ by varying slot gap ($g_s$) are summarized in Fig.2.4. The slot length $l_s$ and width $w_s$ are fixed at $15.9\,mm$ and $1\,mm$, respectively. The resonant frequency shifts down with an increase in $g_s$ alike the previous investigation. The impedance matching at the resonance frequencies are also affected with this variation. By increasing $g_s$, the slot is placed

closer to the feed, affecting the current distribution of it. Hence, a slot close to the feed degrades the antenna matching more than that at far.

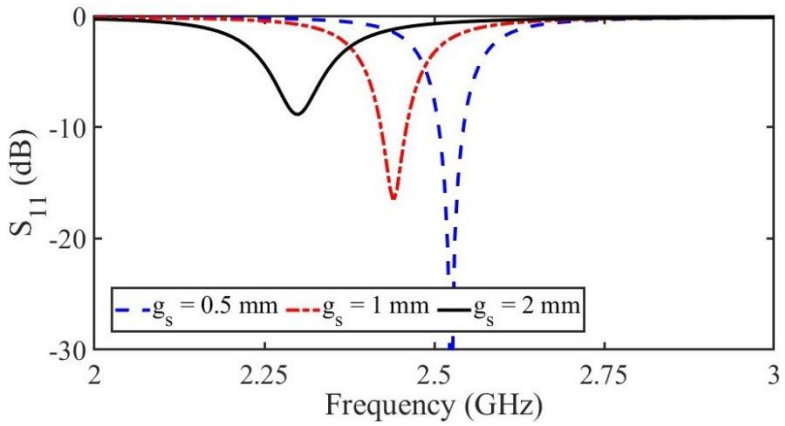


Fig. 2.4: Simulated $S_{11}$ with varying slot width $g_s$.

**Surface Current Distribution**

To understand the working of the slot, surface current distribution of the proposed antenna at $2.45GHz$ is shown in Fig.2.5. It can be observed that the current distribution is maximum around the slot near its perimeter. This explains the lower shift of resonant frequency with an increase in length or width of it. A longer or wider slot offers an elongated current path reducing the operating frequency of it. As, much of the surface current surrounds the slot, its placement near the antenna feed significantly disturbs the overall impedance matching as indicated in previous subsections.

Considering these parametric studies, $l_s = 15.9\,mm$, $w_s = 1\,mm$ and $g_s = 1\,mm$ are considered for the proposed patch with a resonant frequency of $2.45GHz$. The proposed antenna is a miniaturized version of a conventional patch antenna working at the same frequency. The dimension of a conventional rectangular patch antenna considering the same dielectric property is approximately $28.5 \times 36.8\,mm2$ for $2.45GHz$ [4]. The same resonant frequency is observed with the proposed patch of dimension $18.4 \times 13.9\,mm2$ ($0.15\lambda \times 0.11\lambda, \lambda$ is the free space wavelength at $2.45GHz$) having 25% area of the conventional patch. The maximum directivity is slightly sacrificed as a directivity of $5.53dBi$ is observed with the proposed patch instead of the $6.32dBi$ with the conventional patch. The reduction in directivity is due to the increased beam width for the miniaturized aperture of proposed antenna.

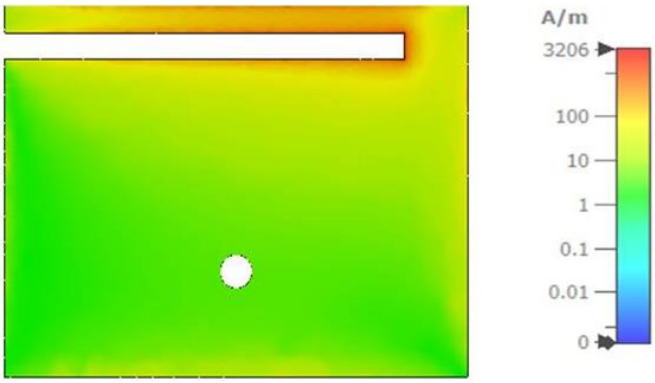


Fig. 2.5: Simulated surface current distribution of the proposed patch at $2.45GHz$

## 2.3. Design of Beam Steering Circuit using Power Divider and Phase Shifter

### 2.3.1. Power Divider

In this work, a $1 \times 8$ power divider circuit is to be designed to power all antennas with equal power levels. This is to excite all antennas simultaneously with a single power source. Different types of standard power division circuits are there such as –

- Wilkinson Power Divider,
- Branch-line coupler,
- Rat-race coupler etc.

These techniques require additional lumped circuit elements to be mounted either for power division operation or to terminate the unused ports with matched impedance. Instead, a simple power division circuit is designed using microstrip lines to serve our requirements. In this section, a simple power division circuit is designed for an equal power division. The $1 \times 8$ Power Divider circuit is implemented using multiple $1 \times 2$ power division units forming a corporate feed network for the antenna arrays.

**Schematic of a $1 \times 2$ power divider circuit**

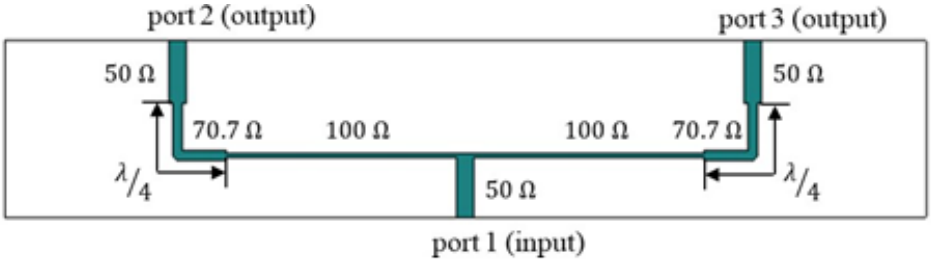


Fig.2.6: Schematic of a $1 \times 2$ Power Divider Circuit

A schematic of a $1 \times 2$ power divider circuit is shown in Fig.2.6. It is designed using microstrip configuration using CST Studio Suite. The input power from port1 is divided into two equal parts between port 2 and port 3. A line impedance of $50\Omega$ is maintained at all ports for matching with the additional circuits. The input power is fed through port 1 which is divided into two equal branches of impedance $100\Omega$. As the input impedance of two $100\Omega$ lines in parallel matches the impedance of port1, all power from the input line is transferred equally among these lines without reflection. But, to match these impedances with those of port 2 and port 3, a quarter-wave transformer is placed in between. A quarter-wave impedance transformer is a piece of transmission line of an impedance $Z_q$ and length $\lambda/4$ ($\lambda$ is the free-space impedance at the operating frequency) to match two different impedanes $Z_1$ and $Z_2$, where $Z_q = \sqrt{Z_1 Z_2}$. Since a $100\Omega$ impedance is to be matched with the port impedances of $50\Omega$, a matching section of $70.7\Omega$ ($\sqrt{100 \times 50}\Omega$) is placed in between.

The width of the line can be calculated by the equation given below

$$\frac{W}{d} = \begin{cases} \frac{8e^A}{e^{2A}-2} & for \ \frac{W}{d} < 2 \\ \frac{2}{\pi}\left[B - 1 - ln(2B-1) + \frac{\epsilon_r - 1}{2\epsilon_r}\left\{ln(B-1) + 0.39 - \frac{0.61}{\epsilon_r}\right\}\right] & for \ \frac{W}{d} > 2 \end{cases} \quad (2.6)$$

Where, $A = \frac{Z_0}{60}\sqrt{\frac{\epsilon_r+1}{2} + \frac{\epsilon_r-1}{\epsilon_r+1}}\left(0.23 + \frac{0.11}{\epsilon_r}\right)$ and $B = \frac{377\pi}{2Z_0\sqrt{\epsilon_r}}$

The effective dielectric constant of any microstrip line is given by the equation below,

$$\epsilon_e = \frac{\epsilon_r+1}{2} + \frac{\epsilon_r-1}{2}\frac{1}{\sqrt{1+12d/W}} \quad (2.7)$$

Where, $W =$ Width of the microstrip line

$d =$ Thickness of the substrate

$\epsilon_r =$ Relative Permittivity of the dielectric

$Z_0 =$ Characteristic impedance of the transmission line

The circuit is designed using microstrip lines on an FR-4 ($\varepsilon_r = 4.3, tan\delta = 0.025$) substrate of thickness $1.57mm$. Considering the operating frequency of $2.45GHz$, widths of the $50\Omega$, $70.7\Omega$ and $100\Omega$ lines are $3.1mm$, $1.6mm$ and $0.72mm$, respectively. Length of the quarter length section is approximately $17mm$. Length of the $50\Omega$ lines does not affect the performance of the power division circuit and can be suitably considered to fit it with the additional circuitry.

**Simulated Results**

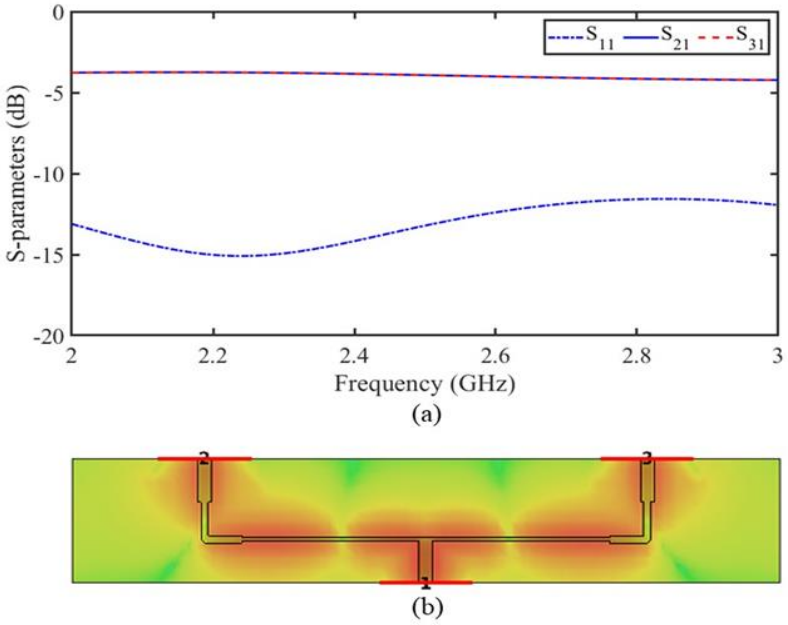


Fig.2.7: Simulated results of a $1 \times 2$ Power Divider (a) S-parameters (a) E-field distribution at $2.45GHz$

The simulated responses of the $1 \times 2$ power division circuit are shown in Fig.2.7. The circuit is simulated using the frequency-domain solver in CST where waveguide ports are connected at the ports exciting the circuit at port1. The simulated $S_{11}$, $S_{21}$and $S_{31}$ are shown in Fig.2.7.(a). Good impedance matching is observed at port1 as $S_{11} < -10dB$ throughout the considered frequency band. The power is equally divided between port2 and port3 as $S_{21}$= $S_{31} = -3.9dB$. Ideally $-3dB$ of power should be delivered at both ports which is reduced due to the loss in the dielectric substrate.

The electric field (E-field) distribution at $2.45GHz$ is shown in Fig.2.7.(b). It can be observed that, the power is divided equally between the ports as the field distributions between the input-output ports are uniform. Hence, the proposed circuit can divide the RF power equally between two ports with good impedance matching at the operating frequency of $2.45GHz$.

**Schematic of $1 \times 4$ and $1 \times 8$ power divider**

It is mentioned earlier that, a $1 \times 8$ power division circuit is to be designed to feed an array of 8 antenna elements. The $1 \times 2$ power divider circuits are cascaded to design $1 \times 4$ Power Divider circuits as shown in Fig.2.8.(a). The circuit is designed using three $1 \times 2$

Power Dividers to form a corporate feed with four outputs. It has port1 as input and port2 to port5 as outputs. Similarly, a $1 \times 8$ Power Divider circuit is designed with seven $1 \times 2$ or two $1 \times 4$ and one $1 \times 2$ power division units as shown in Fig.2.8.(b). It also has port 1 as the input and port 2 to port 9 as output ports. The circuits are designed using and FR-4 substrate of $1.57mm$ hence; different lines of different impedances have the line widths alike the $1 \times 2$ Power Dividers in the previous section.

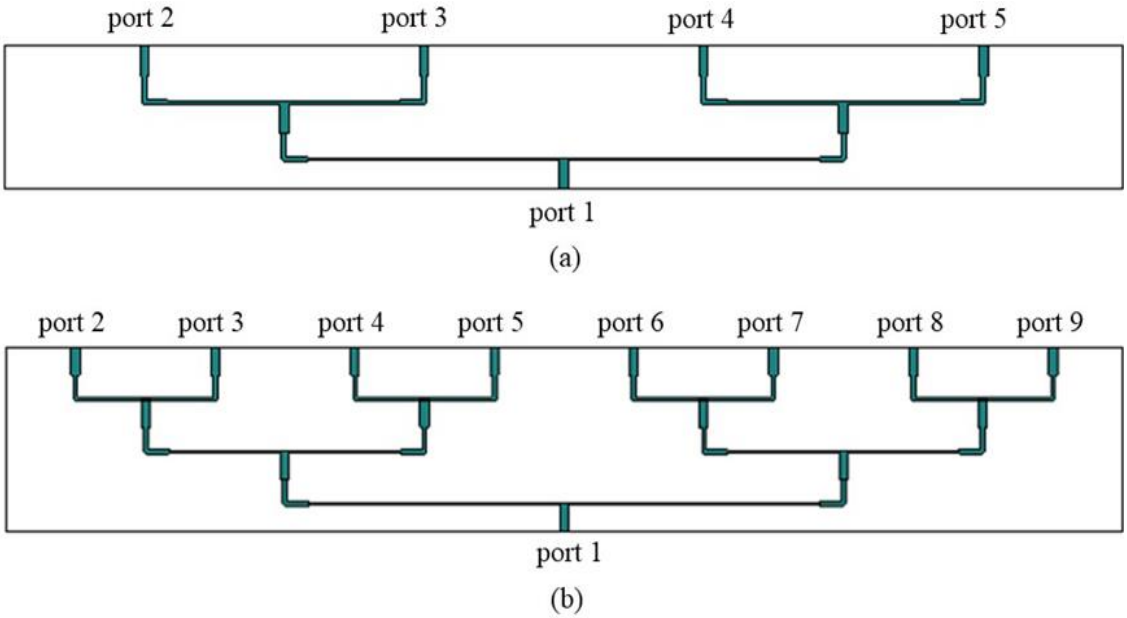


Fig.2.8: (a) $1 \times 4$ and (b) $1 \times 8$ Power Divider Circuits

**Simulated results**

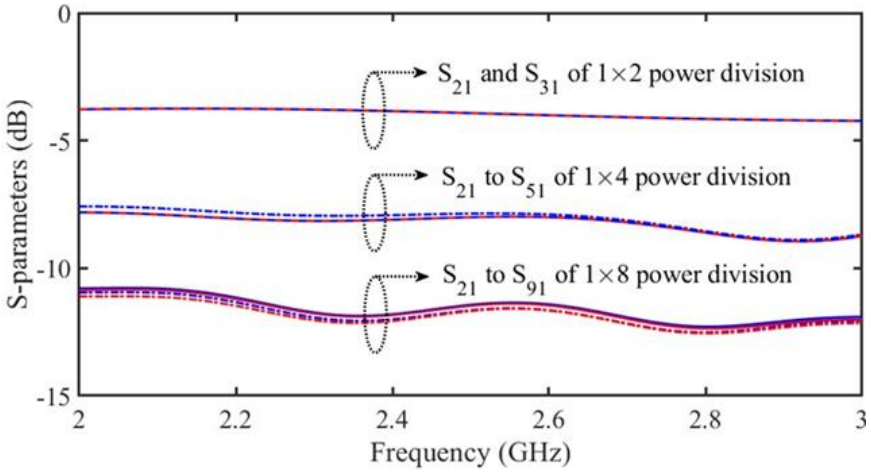


Fig.2.9: Simulated S-parameters for different Power Divider Circuits

The Power Divider Circuits are simulated using CST Studio Suite in frequency domain solver as shown in Fig.2.9. The S-parameters for $1 \times 2$, $1 \times 4$ and $1 \times 8$. It is already mentioned that approximately $-3dB$ power should be transferred between the output ports of a $1 \times 2$ power divider but the output power is reduced due to the dielectric loss in the substrate. Similarly, in a $1 \times 4$ power divider, $-6\,dB$ of power should be delivered at each output port. But, due to dielectric loss approximately $-7.5dB$ of power was delivered at the output ports. Similarly, $-11dB$ of power is observed instead of $-9dB$ at the output ports using a $1 \times 8$ Power Division Circuit.

## 2.3.2. Phase Shifter Circuits

The phase shifter circuits are required to excite an 8-element antenna array with equal power and progressive phase shifts. The Phase Shifter Circuit is designed to investigate the beam steering operation of an antenna array. A simple Power Division and Phase Shifter Network is investigated in this section.

**Schematic of $1 \times 2$ phase shifter**

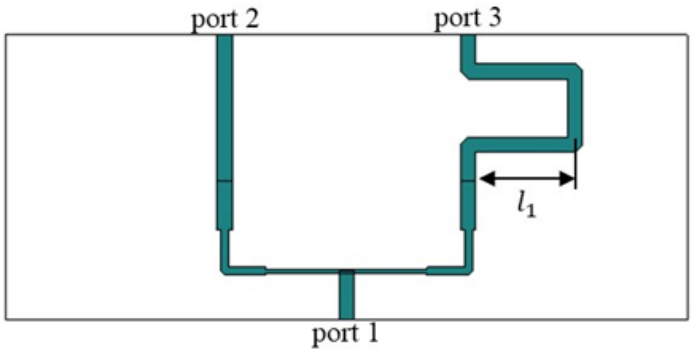


Fig.2.10: Schematic of a $1 \times 2$ Phase Shifter Circuit

A schematic of a $1 \times 2$ Power Divider Phase Shifter Circuit is shown in Fig.2.10. The circuit consists of a power division section as discussed in an earlier section which is followed by a phase shift section. The power from port1 is equally divided between port 2 and port 3 and the phase shift is realized by varying the lengths between the input and output ports. According to the figure, the path length between port1 and port 3 is more than that between port1 and port 2 by a length of $2l_1$. By varying$l_1$, the phase difference between the two output ports can be controlled.

**Simulates Results**

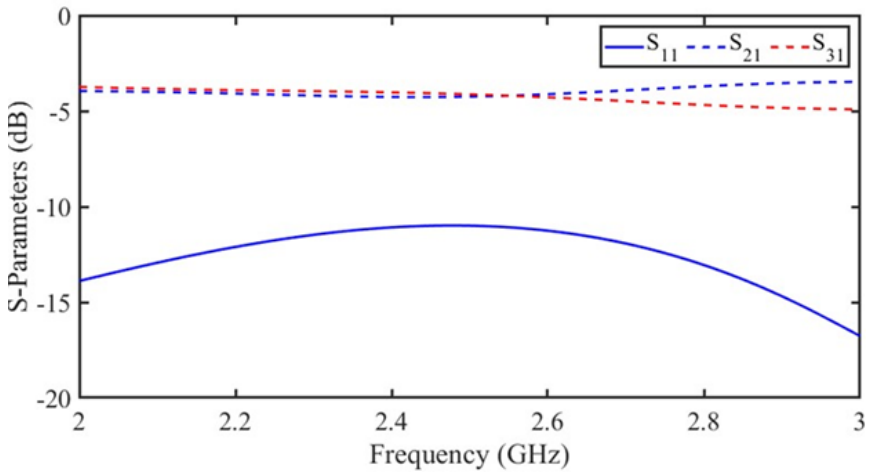


Fig.2.11: Simulated S-parameter magnitudes of the $1 \times 2$ Power Divider Phase Shifter Circuit

The simulated S-parameters magnitudes of the $1 \times 2$ Power Divider Phase Shifter Circuit are shown in Fig.2.11. Good impedance matching is observed at the operating frequency of $2.45GHz$ as $S_{11} < -10dB$ is observed at this frequency point. The power from port1 is also equally divided between the two output ports as $S_{21} = S_{31} = -3.9dB$ is observed in the figure. The reduction in power below $-3dB$ is due to the loss in the dielectric substrate.

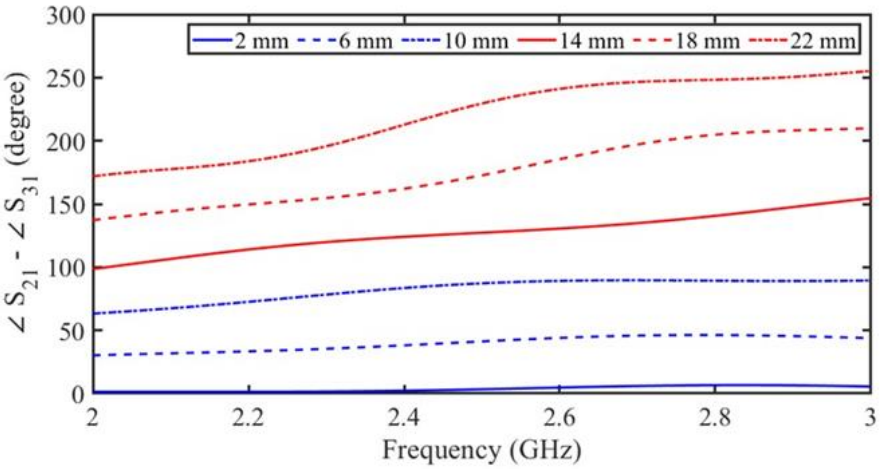


Fig.2.12: Simulated Phase Difference between the output ports of a $1 \times 2$ Power Divider Phase Shifter Circuit for different $l_1$

It is earlier mentioned that the phase difference between the two output ports of a $1 \times 2$ power divider phase shifter circuit can be controlled by varying$l_1$. The phase difference

between the two output ports is denoted by $\angle S_{21} - \angle S_{31}$ and are plotted in Fig.2.12 for different values of $l_1$. The phase difference can be significantly increased by increasing $l_1$ as can be seen in the figure. The phase difference is consistent over the considered frequency range. The phase difference at $2.45GHz$ for different $l_1$ are summarized in Table.2.1, observing a similar trend in the output phase difference.

**Table 2.1: Phase Difference for different $l_1$**

| $l_1$ **(mm)** | 2 | 6 | 10 | 14 | 18 | 22 |
|---|---|---|---|---|---|---|
| $\angle S_{21} - \angle S_{31}$ **(degree)** | 2.8 | 39.7 | 85.6 | 125.9 | 167.5 | 222.7 |

Since the path length between port 1 and port 3 is more than that with port 2, the waves in the latter encounter a higher propagation delay, resulting in positive phase difference between the output ports.

**Schematic of a $1 \times 8$ phase shifter**

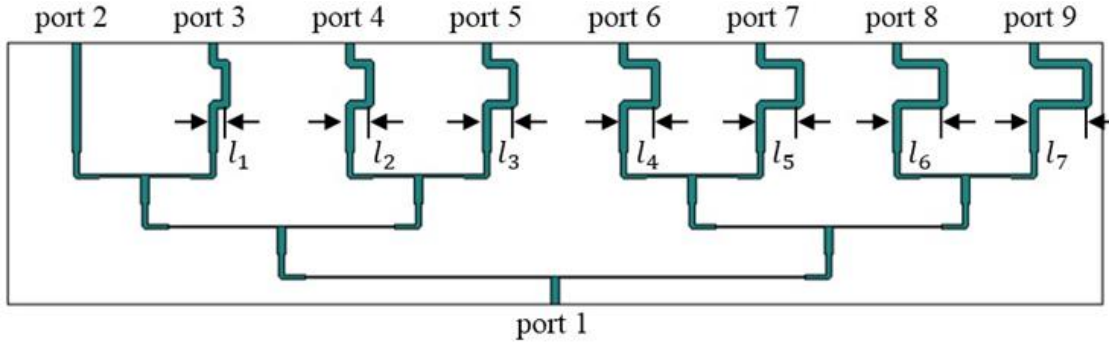


Fig.2.13: Schematic of a $1 \times 8$ Power Divider Phase Shifter Circuit

A schematic of a $1 \times 8$ Power Divider Phase Shifter Circuit is shown in Fig.2.13. It consists of a $1 \times 8$ Power Divider section followed by a Phase Shift Circuits. The Power Division Circuit is same as that in earlier progressive phase shift is implemented from port2 to port9 by adding different lengths of $l_1$to $l_7$ so that,

$$l_i < l_{i+1},\ i\text{=1 to 6.} \qquad (2.8)$$

A length vector is made as,

$$l_v = [l_1, l_2, l_{3,} \dots, l_7] = [4.75, 7.25, 9.5, 11.9, 14.4, 16.8, 20]\ mm \qquad (2.9)$$

is considered for a preliminary investigation. These values are selected in a way so that,

$$\angle S_{21} - \angle S_{31} = \angle S_{31} - \angle S_{41} = \cdots = \angle S_{81} - \angle S_{91}. \quad (2.10)$$

Now, the average phase shift is defined as

$$\Delta\phi = \frac{1}{7}\sum_{i=2}^{8} \angle S_{i1} - \angle S_{(i+1)1} \quad (2.11)$$

The vector is multiplied by the factor $K$ to scale the progressive phase shift and hence $\Delta\phi$ accordingly. The $\Delta\phi$ for different scaling factor are plotted in Fig.2.14. It can be observed that, the average phase shift can be increased by increasing the scaling factor. In other words, by increasing the path lengths in a linear manner, the phase shifts among the ports can also be varied linearly.

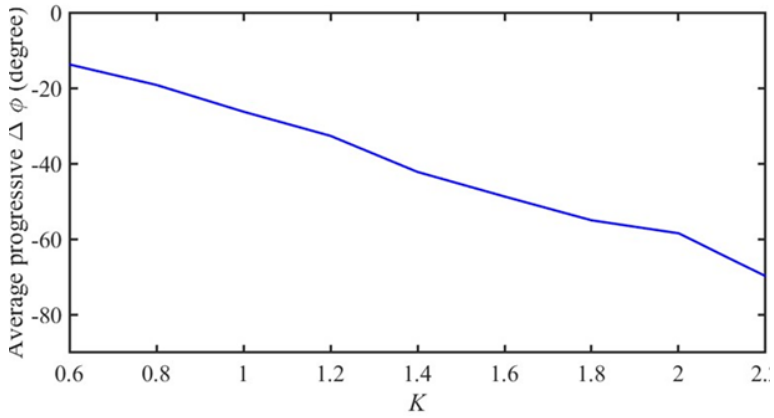


Fig.2.14: Average Phase Shift for different values of $K$

### 2.3.3. Proposed Power Divider and Phase Shifter Circuit with Antenna Array

The Power Divider Phase Shifter Circuit is shown in Fig.2.15(a) (inset). The $50\Omega$ line (width $w_{50}$ = 3.1$mm$) is divided into two $100\Omega$ (width $w_{100} = 0.72\,mm$) lines at each power division point. To match with antenna impedance of $50\Omega$, a quarter wave transmission line of impedance $70.7\Omega$ (length $l_{70} = 17mm$ and width $w_{70} = 1.6\,mm$) is placed in between. Length of the $50\Omega$ lines does not play any role in the design and hence are adjusted according to the placement of the antenna and the underlying circuit. A progressive phase shift from Ant. 1 to Ant. 8 is implemented by varying the length of the phase shifter section as indicated in Fig.2.15(a) (inset). The first two feed lines to Ant. 1 and Ant. 2 are highlighted here. The feed line to Ant. 2 has an additional length of $2l_{ext-1}$ that produces an additional phase shift over the feed of Ant. 1. Therefore, both antennas are fed with signals of identical magnitude of $A_0$ (half of input power$A_i$) but with phases $\phi_1$ and $\phi_2$, respectively. The phase difference of

$\angle\phi_2 - \angle\phi_1$ can be controlled by $l_{ext-1}$. Similar phase shift circuits are used for Ant. 3 to Ant. 8 with different additional lengths. A phase shift ($\phi_v$) vector can be constructed indicating these added lengths from Ant. 1 to Ant. 8 as

$$\phi_v = [0, l_{ext-1}, l_{ext-2}, \ldots\ldots, l_{ext-7}]. \quad (2.12)$$

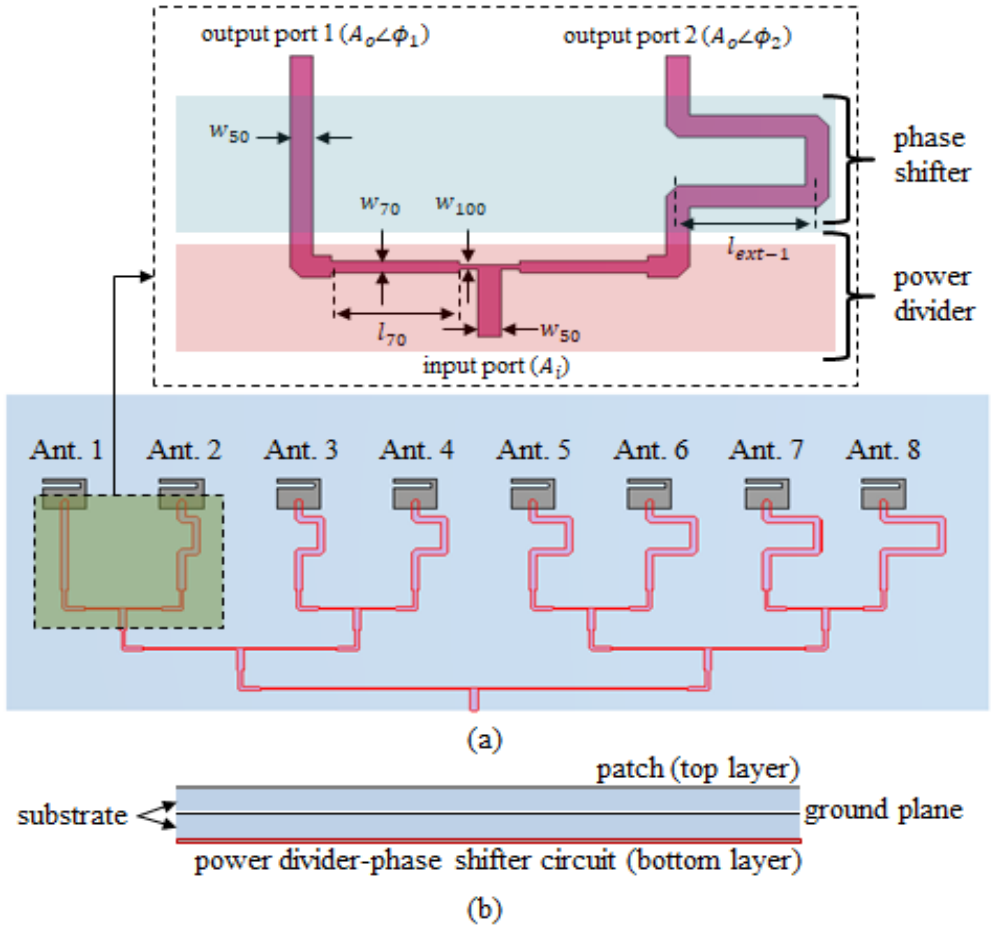


Fig. 2.15: $1 \times 8$ array of the proposed antenna showing (a) top view with a section of power divider-phase shifter circuit (inset), (b) side view showing different layers.

### 2.3.4. Beam Steering with Proposed Antenna

To investigate the beam steering with the proposed antenna, an $1 \times 8$ array is constructed as shown in Fig.2.15 (a). The array is constructed to facilitate the beam steering with the idea of phased array. It also reduces the beam width making usable for steering. The antennas are placed with a periodicity of $50mm$ which is close to $\lambda/2$ at the operating frequency of $2.45GHz$. A corporate feed configuration is used to feed all antennas with a single excitation. Phase shifter circuits are implemented by individually increasing the lengths of each feed line. The antenna and the circuit are printed on the top and bottom sides of a substrate separated by a common ground as shown in Fig.2.15 (b). An FR −4 substrate of

thickness 1.6 mm is placed above and below the ground plane. The feed ends are connected to the antenna using vias through holes in the ground plane.

As the phase shifts are implemented with additional lengths to the feed paths, the antenna beam can only be steered at a certain direction for a fixed $\phi_v$. To vary the steering angle, $\phi_v$ is varied by multiplying it with a constant $mul$ that would change the relative phase differences among the antennas thereby steering the beam at different angles. The normalized radiation patterns on $\phi = 0^\circ$ plane ($zx$ plane) are plotted by varying $mul$ in Fig.2.16. It can be observed that the main beam is guided in boresight ($\theta = 0^\circ$) without any phase shifter when all antennas are excited with same phase. Initially the following $\phi_v$ is considered to be $\phi_v = [0, 4.75, 7.25, 9.5, 11.9, 14.4, 16.8, 19.2]$ (in mm, $mul = 1$), for a squint angle of approximately $12^\circ$. For $= 0.6$, the steer angle of $4^\circ$ is observed due to the reduced phase shifts among the antennas. To squint the beam at a higher angle, $mul = 1.8$ and 2.2 are investigated and the patterns are plotted in the same figure. The beam is guided at approximately $19^\circ$ and $22^\circ$ away from boresight in these cases. Therefore, the $mul$ can be suitably varied to steer the antenna main beam at different angular locations. Further increase in $mul$ can result in an overlapping between the adjacent circuits, hence are avoided in this investigation.

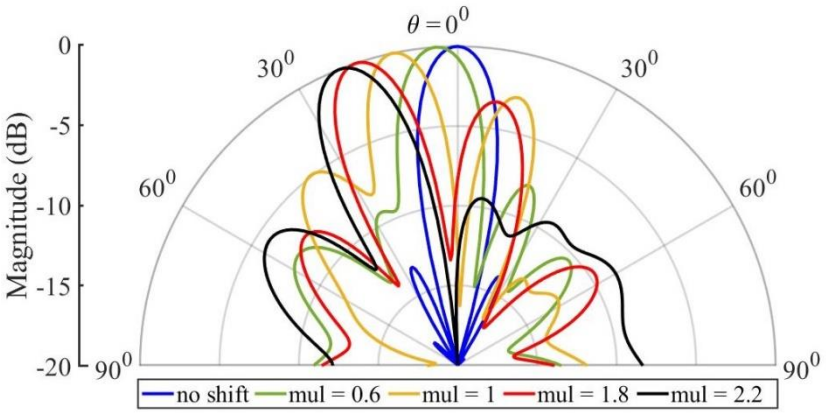


Fig. 2.16: Beam steering with varying $mul$

## 2.4. Summary

A slot loaded miniaturized microstrip patch antenna is designed to work at $2.45GHz$ with an overall dimension of ($0.15\lambda \times 0.11\lambda$, $\lambda$ is the free space wavelength at $2.45GHz$). An $1 \times 8$ antenna array is designed to demonstrate the beam steering using the antenna. A power divider circuit is designed to feed an 8-element antenna array with a single excitation using a corporate feed network. Equal amount of power is delivered at all ports with finite losses due

to the substrate dielectric. Moreover, no lumped circuit elements are required to design the power division network. A phase shifter network is also designed to provide a progressive phase shift in each path of the power divider. The antenna main beam is steered between $\pm 22^{\circ}$ by suitably varying the input phase as demonstrated using simulated results.

# CHAPTER 3

# Design of Smart Tracking System based on proposed Patch Antenna

## 3.1. Introduction

To determine the exact location of the user, a decision making circuit has to be designed to take the decision of the closest antenna patch of the user. In this Chapter, a digital logic circuit is presented which is able to detect the closest antenna patch of the user. For this purpose, the received RF power from the circulator has to be converted to equivalent DC voltage level which can be fed as the input to the digital logic circuit. To convert the received RF power in to equivalent Dc voltage level, a conventional diode based rectenna circuit is designed. The digital logic circuit is designed using op-amp and logic gates to detect the maximum power received to the input of the rectenna or to produce an output to indicate the antenna location receiving the maximum RF.

## 3.2. Design of Rectenna

Rectenna or rectifying antenna is connected at the antenna output to convert the RF power into DC. It is a conventional diode-based rectifier circuit with a load resistor with capacitors in parallel to smoothen the pulsating output. The DC power across the load resistor is generally used for applications like energy harvesting, wireless power transfer etc. In our work, the DC levels from different antennas are extracted to determine the antenna location receiving the maximum RF power. DC voltages are used instead of RF to use simple, cheap, and commercially available circuits for magnitude comparison. A general block diagram of conventional rectenna circuit is given in Fig.3.1.

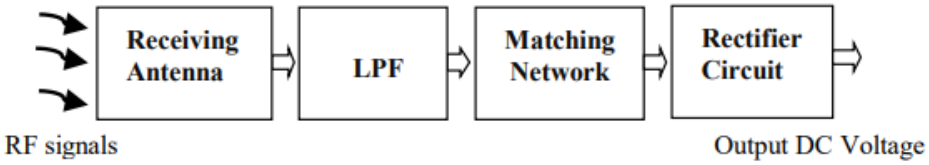


Fig.3.1: General rectenna structure

### 3.2.1. Schematic of Rectenna

A schematic of the proposed rectenna circuit is shown in Fig.3.2. It is designed using Keysight ADS which is a well-known EM simulator for RF systems. The circuit consists of an SMS7630 Schottky diode suitable for ISM band applications with a series load resistor $R_L$. A capacitor of $10\,nF$ is connected in parallel to the load for filtering. The circuit is excited with a tone of $2.45GHz$ of magnitude $p_{in}$ in $dBm$. Two power probes are connected at the input and output of the rectifier to observe the power levels at those points. An impedance matching circuit is employed at the input of the rectenna to match the line impedance of $50\Omega$ with that of the diode.

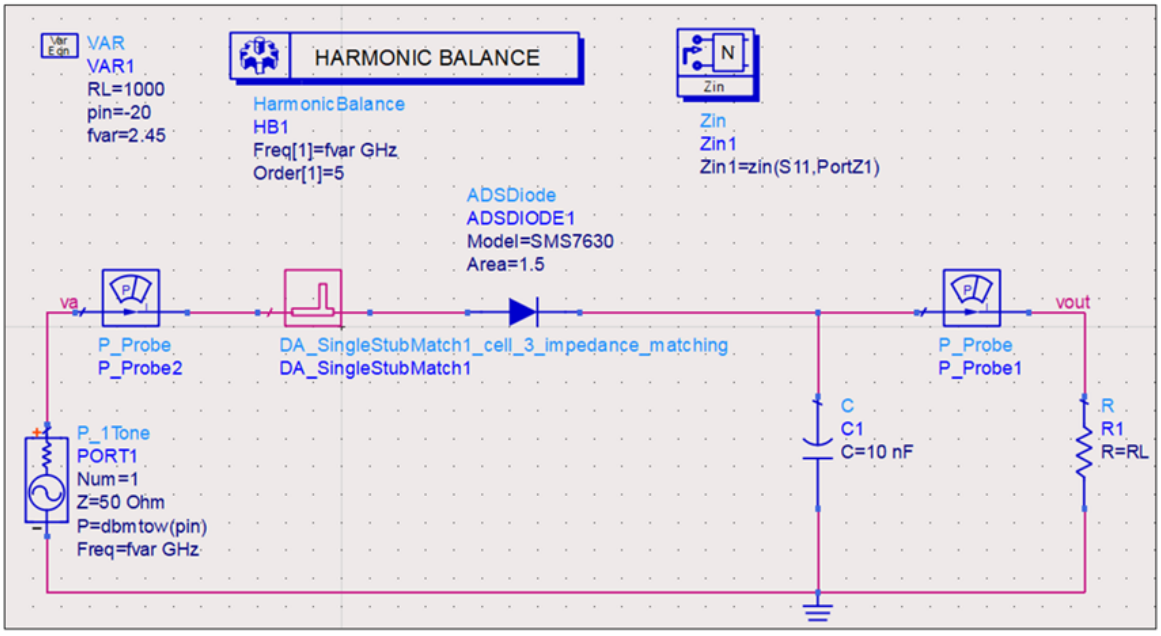


Fig. 3.2: Schematic of Rectenna Circuit

### 3.2.2. Simulated Investigation

The simulations are carried out using the harmonic balance simulator which is a frequency domain numerical technique used to analyze nonlinear circuits. It can be used to determine the power levels at the tone as well as at its harmonics often found in practical sources and circuits. Hence to analyze any active circuit like an amplifier, mixer, modulator etc., consisting of diodes and transistors, harmonic balance can be used.

Initial investigations are carried out by setting $R_L = 1\,K\Omega$ without the impedance matching circuit. The efficiency (η) for different $p_{in}$ are shown in Fig.3.3.

$$\eta = \frac{V_{DC}^2}{P_{in} \times R_L} \times 100 = \frac{p_{in}}{p_{out}} \tag{3.1}$$

where, $p_{out(DC)}$ is the DC power present across the load. $p_{in}$ is the received RF input power and $R_L$ is the resistive load.

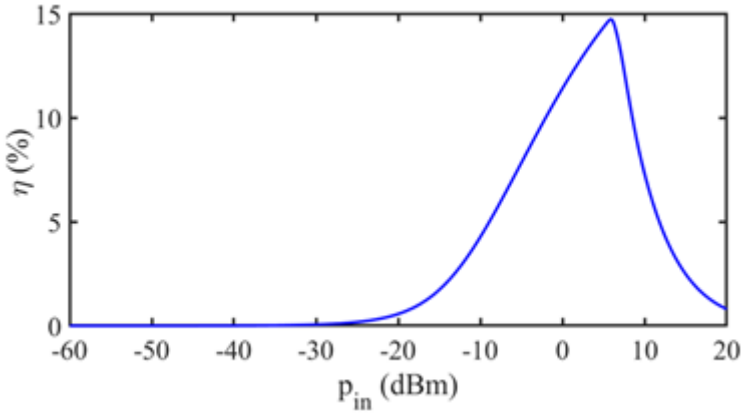


Fig.3.3: η for different $p_{in}$ without matching circuit

A maximum of 15% efficiency is observed with an input power of approximately 5 $dBm$. For lower input powers, the diode may not be turned ON resulting in less output power and low efficiency. Once the diode is turned ON, its impedance changes with input power due to its non-linear behaviour, resulting in an impedance mismatch and reduction in output power, thereby reduce the overall efficiency. An input impedance of approximately $47 - j303\Omega$ is observed at the input of the circuit. The load resistor can also be varied to maximize the efficiency of the rectifier.

A single stub matching circuit is placed in series at the input side of the rectifier as shown in Fig.3.4. The Impedance Matching tool in the simulator is used to design the matching section. This matching ensures the maximum power transfer from source to diode for rectification. After input matching, the load resistor $R_L$ is varied to maximize the efficiency as shown in Fig.3.4.

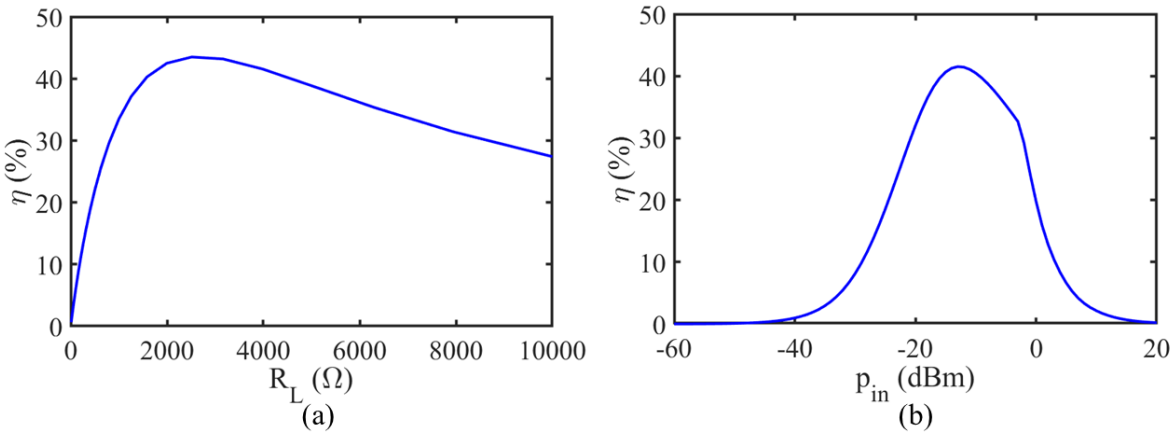


Fig.3.4: (a) η for different $R_L$, (b) variation in $R_L$ with $p_{in}$ with input matching and optimized $R_L$

The efficiency increases sharply with the load resistor and gradually decreases after the maximum value. Maximum efficiency of approximately 42% is observed with $R_L$= 2500Ω as shown in Fig.3.4.(a). With this load resistor, the maximum power is converted into DC improving the efficiency, significantly.

In another simulation, the input power is varied considering the matching circuit and $R_L = 2500\Omega$. The maximum efficiency of 42% is observed with $p_{in} = -13dBm$. The efficiency peak is obtained with much lower input power than that without the matching network. This also proves the usefulness of the matching network that ensures more power to be transferred to the diode, by turning it ON a much lower input power. Further increase in power results in a change in diode impedance and a reduction in the efficiency as shown in Fig.3.4.(b). Hence, the matching circuit can be optimized for other input power levels which is currently beyond the scope of this work.

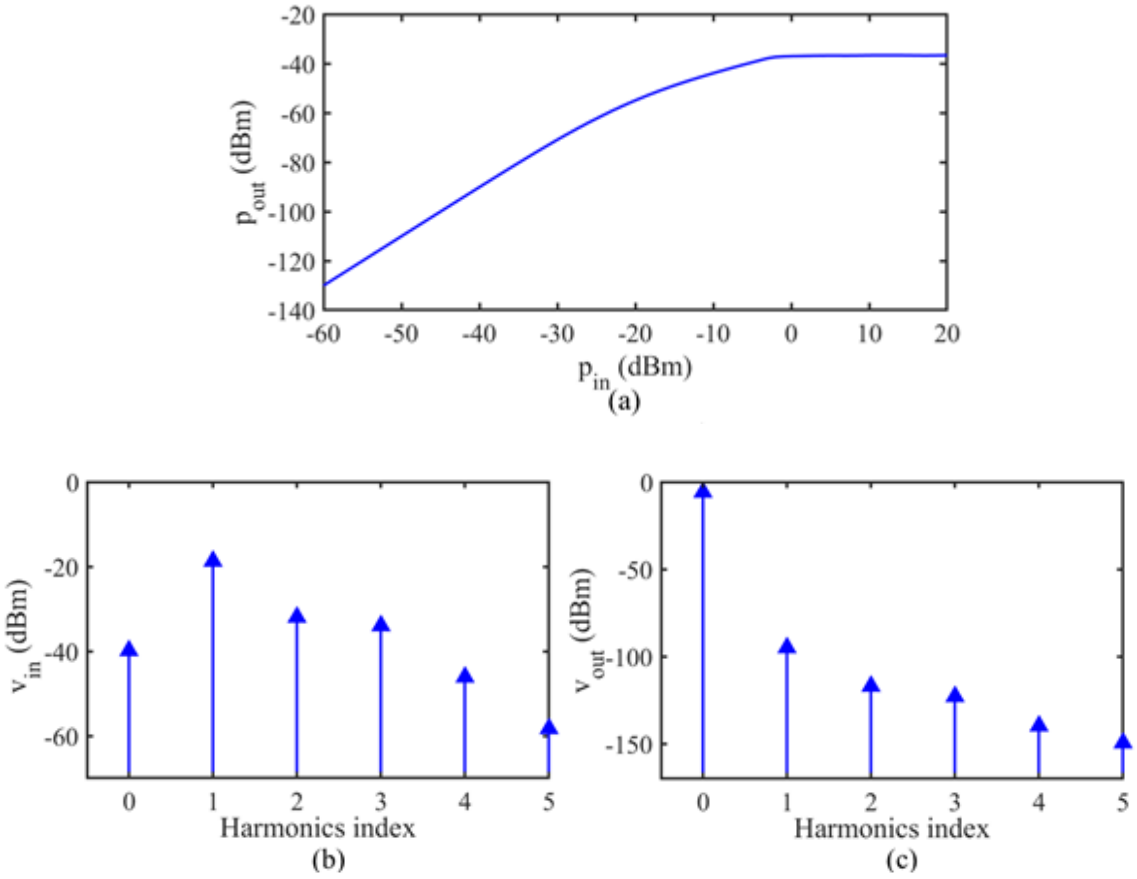


Fig.3.5: (a) Output DC Power for different input power levels. The spectrum of (b) Input Voltage and (c) Output Voltage

The output DC power for different input powers is shown in Fig.3.4. The output power increases linearly with input reaching the saturation at a higher level. Saturation of output power level resulted in the reduction in efficiency with higher values of $p_{in}$. The linear relation between the input and output can be useful to simplify the comparison operation in the following section of rectenna.

The tone and harmonics of the input ($v_{in}$) and output ($v_{out}$) voltages are plotted in Fig.3.4.(b) and (c), respectively. The $0^{th}$ harmonic represents the DC component where the index 1 indicates the tone at $2.45GHz$. Other harmonic indexes represent the higher-order harmonics of the tone. The input voltage is high at $2.45GHz$ and those at other indexes are significantly low as shown in Fig.3.4.(b). On the contrary, the DC voltage level is highest at the output and those at other harmonic indexes are significantly low. It also shows the effectiveness of the proposed rectenna circuit which can convert the RF into DC with good overall efficiency.

## 3.3. Design of Maximum Power Detection logic

### 3.3.1. Detection Logic

At the rectenna output, different DC voltage levels are received as it converts the RF energy to equivalent DC. Now, these DC voltages are compared to detect or identify the maximum DC level from the rectenna output and the corresponding antenna. As the antenna closest to the user receives the maximum RF due to the shortest distance, the corresponding DC level at the rectenna output will be the maximum. Therefore, by identifying the corresponding channel with maximum DC output, the antenna closest to the user can be determined. The magnitude or phase comparison at the RF domain requires additional expertise that can be simplified by using the DC domain. Objective of the DC circuit is to produce an output to indicate the antenna location receiving the maximum RF.

### 3.3.2. DC Level Comparison

Block diagram of the maximum power detection circuit is shown in Fig.3.5. In consists of two different sections. In the first section, all RF levels are compared to each other using op-amp based comparator circuit producing digital signals at its output. From the working of a comparator circuit it is known that, the op-amp output will be set to $+V_{ee}$ or $-V_{ee}$ based on the input magnitudes at its inverting and non-inverting terminals. The rectenna outputs can range between any random magnitudes due to the random reception of RF power through the

antennas. Therefore, the random DC levels must be mapped into digital levels before feeding them into the digital logic. The comparator arrangement compares all rectenna outputs with each other mapping them between $+V_{ee}$ or $-V_{ee}$. The one-to-one comparison requires an $N(N+1)/2$ number of comparators resulting 28 op-amps for 8 $(N)$ input levels.

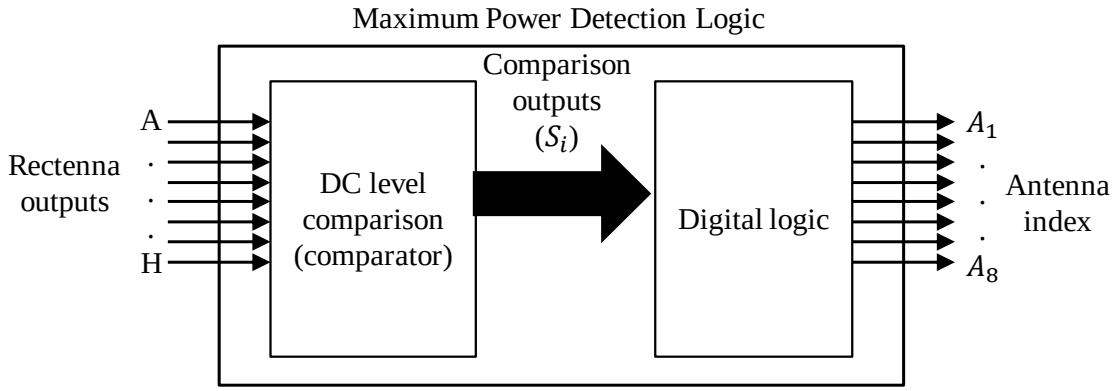


Fig.3.6: Block diagram of Maximum Power Detection Circuit

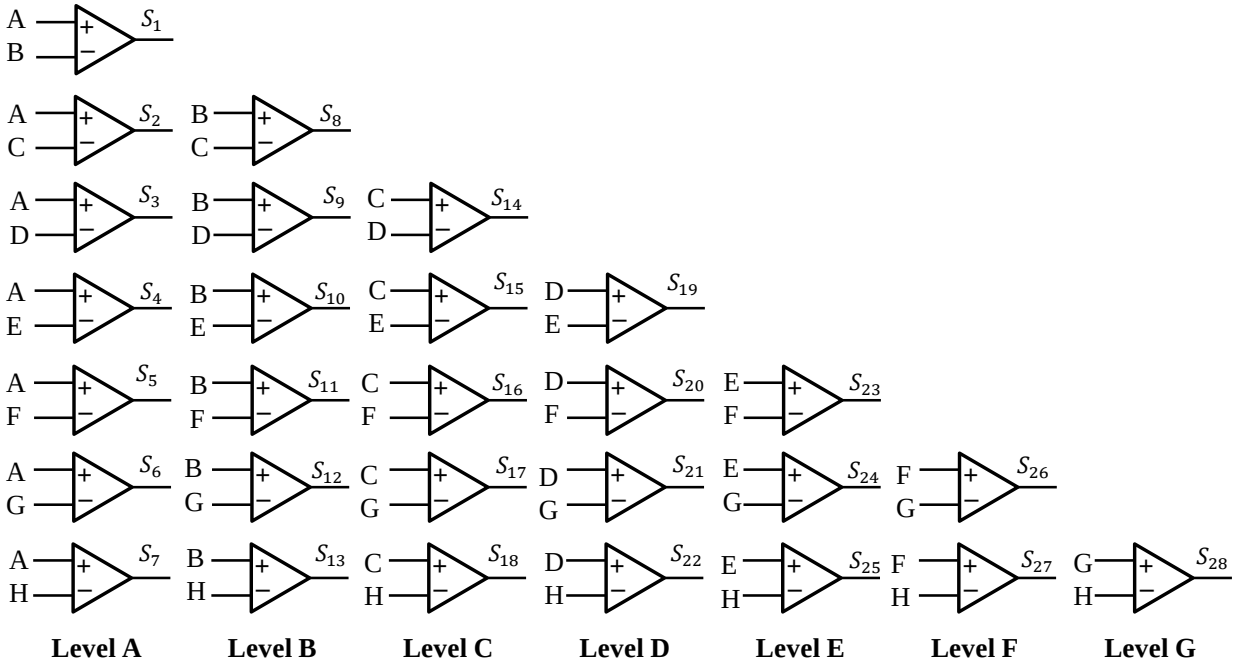


Fig.3.7: Different levels for the comparator arrangement for DC level comparison

Input of the DC level comparator is marked as A to H indicating the outputs from rectenna 1 to rectenna 8, respectively. These are used to generate a set of 28 digital signals indicated by $\{S_i\}$ in Fig.3.5. Schematic of the comparator arrangement with different levels using the op-amps indicating the corresponding inputs and outputs are shown in Fig.3.6. The entire set is divided into seven levels in represent the comparison levels sequentially. In Level 1, A is compared with B to H and the outputs are marked as $S_1$ to $S_8$. In level 2, B is

compared with C to H and the outputs are marked as $S_9$ to $S_{15}$. This is continued till level 8 indicating the last output by $S_{28}$. Height of the levels reduces to avoid the comparison between the same pair at different levels. All $\{S_i\}$ are mapped between the $+V_{ee}$ and $-V_{ee}$ values which are fed to the digital logic as shown in Fig.3.7.

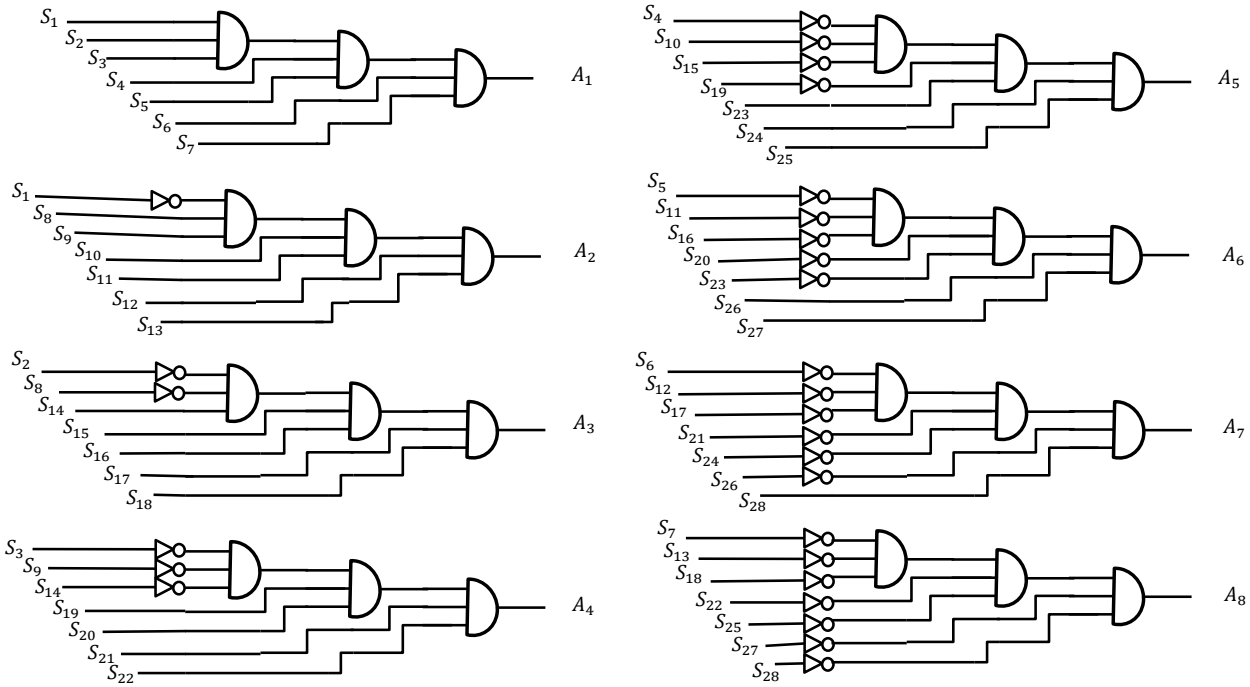


Fig.3.8: Implementation of the digital logic using 3-input AND gate

### 3.3.3. Digital Logic

The $\{S_i\}$ is used to indicate the antenna receiving the maximum RF. The system combines the 28 inputs and generates a 8-bit output to index the antenna as shown in Fig.3.8. Following is the truth table of the proposed digital circuit.

**Truth Table**

| **Inputs** | | | | | | | Outputs | | | | | | | |
|---|---|---|---|---|---|---|---|---|---|---|---|---|---|---|
| | | | | | | | $A_1$ | $A_2$ | $A_3$ | $A_4$ | $A_5$ | $A_6$ | $A_7$ | $A_8$ |
| $\boldsymbol{S1}$ | $S2$ | $S3$ | $S4$ | $S5$ | $S6$ | $S7$ | 1 | 0 | 0 | 0 | 0 | 0 | 0 | 0 |
| $\overline{\boldsymbol{S1}}$ | $S8$ | $S9$ | $S10$ | $S11$ | $S12$ | $S13$ | 0 | 1 | 0 | 0 | 0 | 0 | 0 | 0 |
| $\overline{\boldsymbol{S2}}$ | $\overline{S8}$ | $S14$ | $S15$ | $S16$ | $S17$ | $S18$ | 0 | 0 | 1 | 0 | 0 | 0 | 0 | 0 |
| $\overline{\boldsymbol{S3}}$ | $\overline{S9}$ | $\overline{S14}$ | $S19$ | $S20$ | $S21$ | $S22$ | 0 | 0 | 0 | 1 | 0 | 0 | 0 | 0 |
| $\overline{\boldsymbol{S4}}$ | $\overline{S10}$ | $\overline{S15}$ | $\overline{S19}$ | $S23$ | $S24$ | $S25$ | 0 | 0 | 0 | 0 | 1 | 0 | 0 | 0 |
| $\overline{\boldsymbol{S5}}$ | $\overline{S11}$ | $\overline{S16}$ | $\overline{S20}$ | $\overline{S23}$ | $S26$ | $S28$ | 0 | 0 | 0 | 0 | 0 | 1 | 0 | 0 |
| $\overline{\boldsymbol{S6}}$ | $\overline{S12}$ | $\overline{S17}$ | $\overline{S21}$ | $\overline{S24}$ | $\overline{S26}$ | $S28$ | 0 | 0 | 0 | 0 | 0 | 0 | 1 | 0 |
| $\overline{\boldsymbol{S7}}$ | $\overline{S13}$ | $\overline{S18}$ | $\overline{S22}$ | $\overline{S25}$ | $\overline{S27}$ | $\overline{S28}$ | 0 | 0 | 0 | 0 | 0 | 0 | 0 | 1 |

**Boolean expression**

According to the truth table, the required Boolean expressions are -

$A_1 = S1.S2.S3.S4.S5.S6.S7$

$A_2 = \overline{S1}\,.S8.S9.S10.S11.S12.S13$

$A_3 = \overline{S2}\,.\overline{S8}\,.S14\,.S15.S16.S17.S18$

$A_4 = \overline{S3}\,.\overline{S9}\,.\overline{S14}\,.S19\,.S20\,.S21\,.S22$

$A_5 = \overline{S4}\,.\overline{S10}\,.\overline{S15}\,.\overline{S19}\,.S23\,.S24\,.S25$

$A_6 = \overline{S5}\,.\overline{S11}\,.\overline{S16}\,.\overline{S20}\,.\overline{S23}\,.S26\,.S28$

$A_7 = \overline{S6}\,.\overline{S12}\,.\overline{S17}.\overline{S21}\,.\overline{S24}\,.\overline{S26}.S28$

$A_8 = \overline{S7}.\overline{S13}.\overline{S18}.\overline{S22}.\overline{S25}.\overline{S27}.\overline{S28}$

**Simulated Circuit**

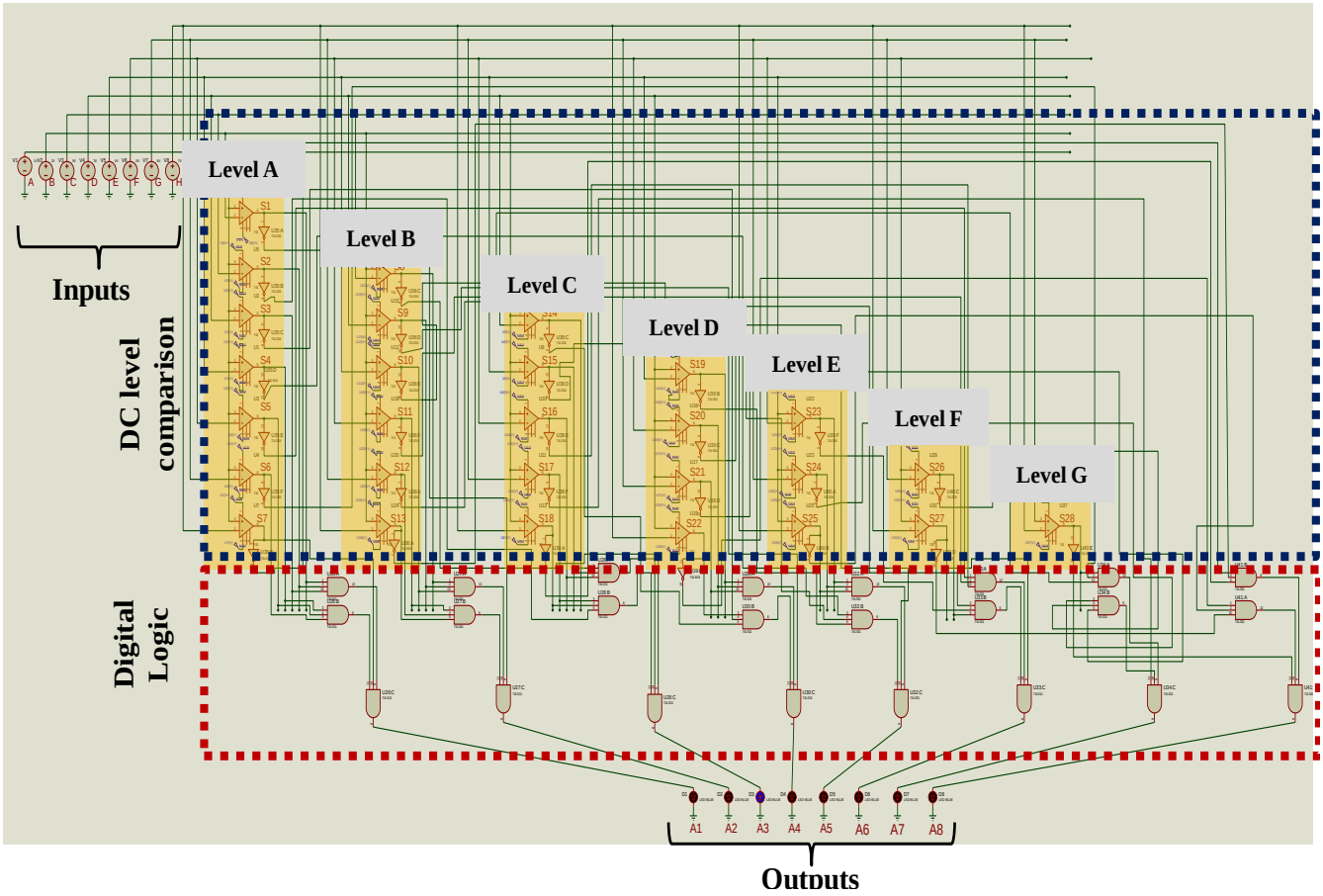


Fig.3.9: Simulated Digital Logic Circuit in Proteus

**Simulated output**

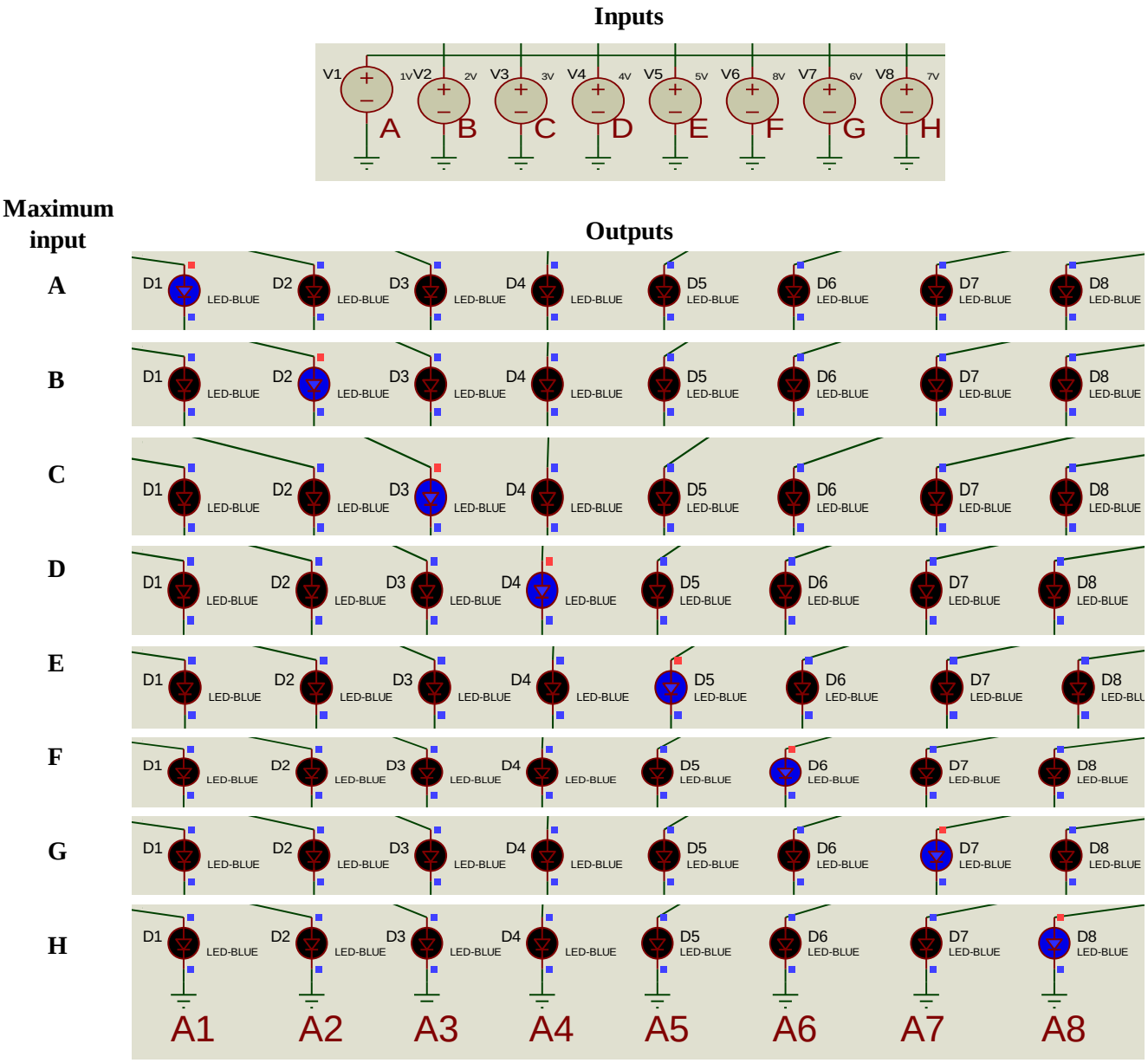


Fig.3.10: Simulated outputs for different inputs

The proposed digital circuit is simulated in Proteus 8.1 which is a hybrid simulator for analog and digital circuit simulation. The DC level comparison circuit is encircled with dark dotted lines, highlighting the levels with a different colour. The op-amp IC741 model is used in the comparator circuit as shown in Fig.3.9. This section is followed by the digital control section consisting of the digital gates. Three input AND gate IC 7411 and NOT gate IC 7404 are used in the circuit. The inputs are marked with A to H are set to different DC voltage levels replicate the rectenna outputs. The circuit generates an eight bit input indexing the antenna receiving the maximum RF power. To indicate the output, blue LEDs are connected

at the outputs as shown in Fig.3.10. The ON and OFF states are indicated by the black and blue colours of the LED. Hence, an LED turns blue when the corresponding input is the maximum. From the index of the glowing LED the antenna index is determined between $A_1$ and $A_8$ as shown in Fig.3.10.

## 3.4. Summary

A single diode based rectenna geometry is designed to convert the input RF into DC output voltages. The load resistor is optimized to maximize the rectenna output. For an input voltage of approximately $13dBm$, a maximum of $42\%$ efficiency is observed. Using numerical study, it is shown that the RF power centred on the fundamental harmonics is successfully transferred into the $0^{th}$ harmonic or DC component. The rectenna circuit is followed by a maximum power detection network that indicates the antenna receiving the maximum RF power. An op-amp based comparator circuit is designed to compare the input analog voltages to generate the digital outputs. These digital levels are used to calculate the antenna index using a digital logic. The working of the proposed circuit is validated by the relevant simulation studies as discussed in Section 3.2.2 and 3.3.3.

# CHAPTER 4

# Proposed Smart Tracking System using Beam Steering Technique

## 4.1. Introduction

This chapter deals with the transmitting and receiving section of the proposed smart tracking system. The idea of determining the user location based on the received RF signal by the patch array is discussed. Circulators are investigated as the decoupling circuit between the transmitting and receiving RF chains.

## 4.2. Detection of Receiver Location

The received signal magnitudes at the output of each antenna element of the 1x8 array are analyzed to detect the location of the user location relative to the array. The user location is used to steer the main beam towards the user for an effective utilization of the radiated power. Variation in the received power is investigated in the following section using a $1 \times 2$ array to understand the effectiveness of the proposed approach.

**Receiver Power for Different User Locations**

As mentioned earlier, an $1 \times 2$ antenna array is designed to detect the user location at the far field. A simple half wavelength dipole antenna is placed in front of the patch array to represent the user location. The dipole is used as a transmitter and its location is varied at along the z-axis (d) and x-axis ($x_{shift}$) as shown in Fig.4.1. The patch array kept at a fixed spatial location receives the EM power transmitted by the dipole. The dipole is excited with a lumped port denoted by Port 1 and the radiated power is detected using waveguide ports at Port 2 and Port 3, respectively.

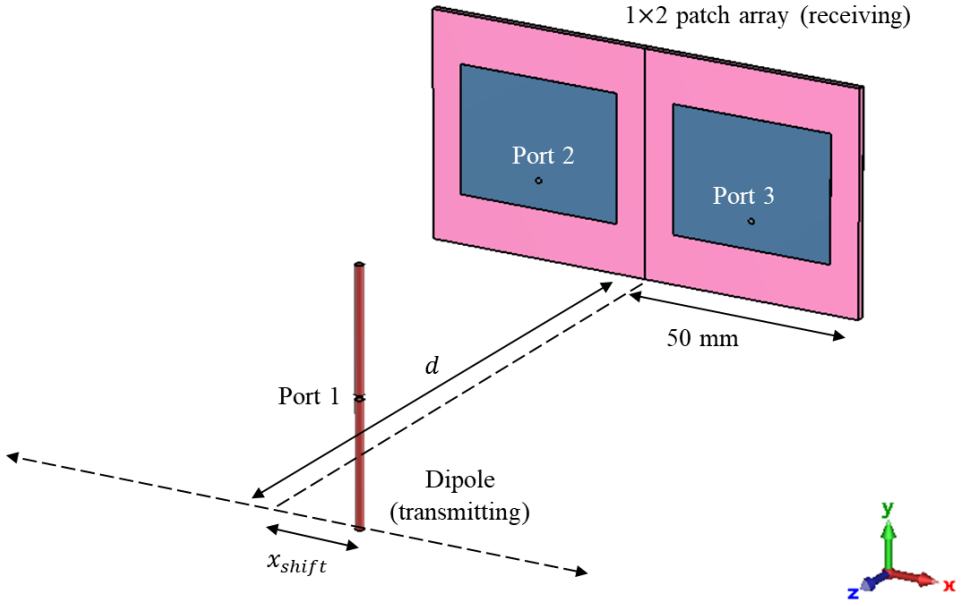


Fig.4.1: Schematic of dipole and $1 \times 2$ array of patch antenna to simulate different user location.

**Variation in d**

In the first investigation, the distance between dipole and array 'd' is varied by setting $x_{shift} = 0$ mm. Since the dipole is moved along the z-axis, its Euclidean distance from individual patch antenna remains the same. The simulated s-parameters for different values of d are summarized in Fig.4.2 over the considered frequency range and, $S_{21}$ and $S_{31}$ are used to determine the received power through port 2 and port 3 considering Port 1 as the transmitter. Since the antennas are designed to work at $2.45GHz$, the received power is maximum at this frequency for any configurations. The S-parameter values reduce linearly with an increase in d due to the increase in the free space path loss. The $S_{21}$ and $S_{31}$ at each distance overlaps as the dipole maintains the same Euclidean distances from each patch in the array. The simulated responses at $2.45GHz$ are also plotted for different d as shown in Fig.4.2 (b). It can

be observed that, the received power reduces linearly as the distance between the dipole and patch array increases. Therefore, it is understood that, if the received power are equal in magnitude and scales linearly with time, the user is moving along the array axis without any lateral movement. Selection of d is critical since it should be sufficiently large enough to ensure the farfield of individual radiator. Considering the antenna dimensions, the farfield distances are approximately $50mm$ ($2D^2$/lambda) for all antennas.

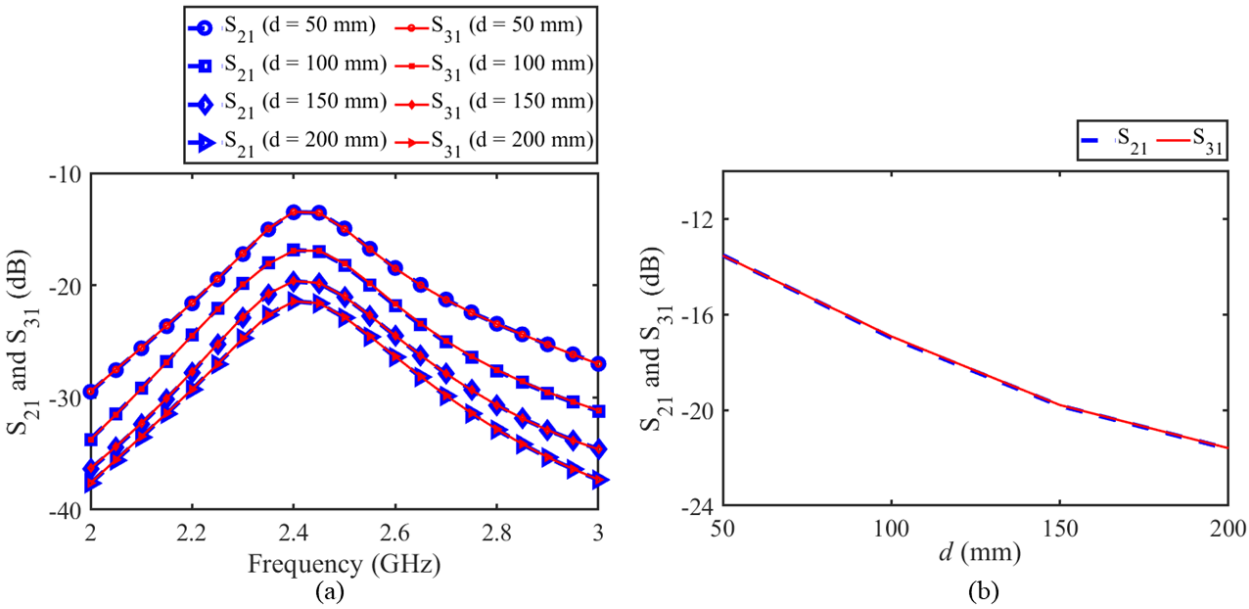


Fig.4.2: (a) The simulated responses for different values of d. (b) $S_{21}$ and $S_{31}$ for different values of d at $2.45GHz$

**Variation in $x_{shift}$**

Variation in $x_{shift}$ is used to determine the lateral movement of the user relative to the axis of the array. The $S_{21}$ and $S_{31}$ for different $x_{shift}$ at $2.45GHz$ are plotted in Fig.4.3 with $d = 50\,mm$. The positive and negative values of $x_{shift}$ are used to indicate the user movement towards the positive and negative direction of x-axis, respectively. The received power at power 2 is maximum for $x_{shift} = -37.5$ mm, when the distance between the dipole and left patch (Port 2) is minimum. A significantly low and $S_{31}$ is observed at this point since, the distance between the transmitter and right patch (port 3) is significantly high. On the contrary, the maximum and $S_{31}$ is observed for $x_{shift} = 37.5$ mm where $S_{21}$ is significantly low. Both responses overlap for $x_{shift}$ = 0 when the dipole is exactly on the axis of the array as shown in Fig.4.3. Therefore, from this investigation, it can be understood that,

the difference in received power indicates a lateral movement of the user about the antenna array and the location can be correctly determined from the magnitudes of the s-parameters.

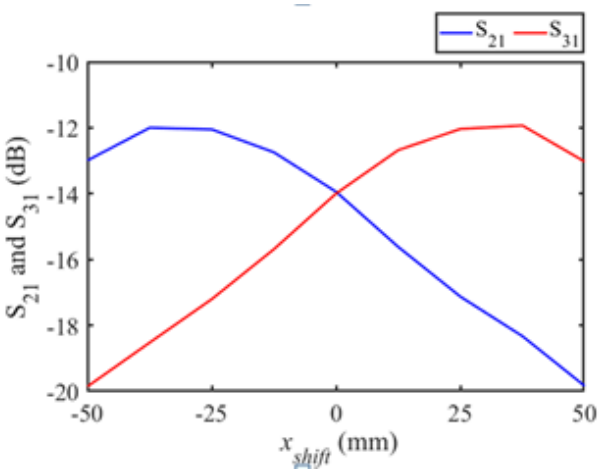


Fig.4.3: $S_{21}$ & $S_{31}$ for different values of $x_{shift}$ at $2.45GHz$

## 4.3. Design of Circulator

A circulator or decoupling circuit maintains a unidirectional flow of EM power in a circuit. Conventionally, it is a three-port network used at the junction of a transceiver unit. It connects the transmitter side with the antenna to transmit power from circuit to antenna. On the contrary, it connects the antenna to the receiving side during reception. It also prevents the flow of direct power between the transmitting and receiving sections.

A matched three-port reciprocal network can be used as a circulator as discussed in [74]. Ferrite materials are conventionally used to introduce non-reciprocity in such networks. The s-parameter of a circulator is

$$[S] = \begin{bmatrix} S_{11} & 0 & S_{13} \\ S_{21} & S_{22} & 0 \\ 0 & S_{32} & S_{33} \end{bmatrix} \quad \text{or} \quad [S] = \begin{bmatrix} S_{11} & S_{12} & 0 \\ 0 & S_{22} & S_{23} \\ S_{31} & 0 & S_{33} \end{bmatrix}$$

### 4.3.1. Design of a ferrite circulator

A ferrite-based circulator is one of the conventional circulator circuits with a ferrite bead that makes the overall geometry non-planer. It is typical 3-port network having input, output and decoupled port. The ferrite introduces non reciprocity in the network facilitating an unidirectional flow of EM waves without any loss with all ports matched. For example, the incident wave at Port 1 is coupled to port 2, whereas port 3 remains isolated. Similarly, a wave incident in port 2 is coupled to port 3 and port 1 is isolated, and so on. In Y-Junction

ferrite circulators, rectangular waveguide or stripline are commonly used. Here, the design Y-Junction ferrite stripline circulator for $2.45GHz$ operation is investigated.

**Schematic**

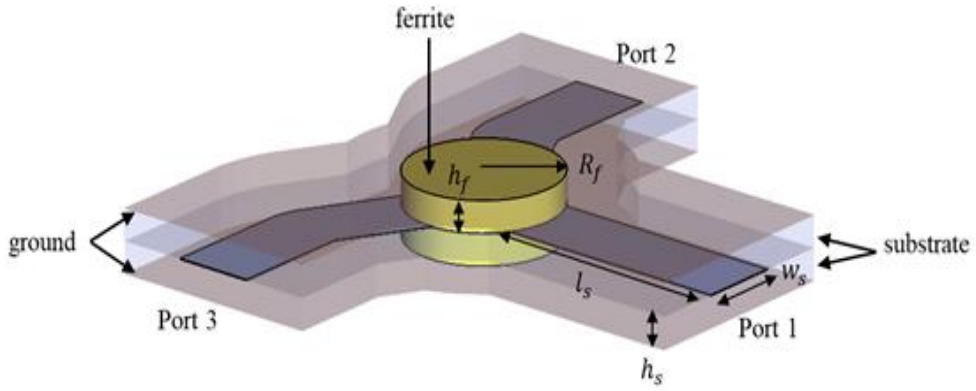


Fig.4.4: Schematic of the proposed circulator

The geometry of the stripline circulator is shown in Fig.4.4. It consists of two ferrite planar disk resonators separated by a metal disk conductor symmetrically coupled by three conductor lines placed at 120° to each other. An Air (epsilon = 1) medium is considered as the dielectric substrate. For this design, the ferrite material was chosen first, and then the other parameters were calculated based on chosen parameters of the ferrite. Ni-Zn ferrite material was used for the performance simulation. The design parameters of the ferrite are shown in Table 4.1.

**Table 4.1: Design parameters of the ferrite**

| **Property** | **Values** |
|---|---|
| Dielectric Constant($\varepsilon_r$) | 12.4 |
| Saturation Magnetization($4\pi M_s$) | 3200 $Gauss$ |
| Resonance Linewidth($\Delta H$) | 200 $Oe$ |
| Dielectric Loss ($\tan\delta$) | 0.0006 |
| Lande G | 2.2 |

The radius of ferrite disk was calculated using Eq.4.1 for the center frequency of $2.45GHz$.

$$kR_f = x \tag{4.1}$$

Where,

$$k = \frac{2\pi f \sqrt{(\varepsilon_{r.ferrite}\, \mu_{eff,ferrite})}^{1/2}}{c} \quad (4.2)$$

$R_f$ is the radius of the ferrite disk, $k$ is the wave number, and $x$ x is the first circulation conditions for using a disk resonator. To find $k$, with the ferrite dielectric constant ($\varepsilon_r$) of 12.4, the ferrite effective permeability ($\mu_{eff}$) must be calculated first,

Where,

$$\mu_{eff}=(\mu^2 - k^2/\mu) \quad (4.3)$$

For the width of conductor lines ($w_s$) should not be very small, as it will lead increased losses. The width of conductor line is calculated using the following equation (4.4):

$$w_s = 2R_f\, Sin\, \psi n \quad (4.4)$$

The length of conductor transmission line is calculated using the quarter wavelength formula as given below:

$$l_s = \frac{\lambda}{4} = \frac{c}{f\sqrt{\varepsilon_r}} \quad (4.5)$$

Using (4.4), the width of strip conductor is calculated, resulting $w_s = 5.65mm$. The calculated length of conductor transmission line section using (4.5) is $l_s = 7mm$. Another parameter that is important to find is the thickness of the ferrite. The ferrite thickness is calculated using analytical line impedance for stripline structure to meet the matching impedance of $50\Omega$. The thickness was found to be close to $h_f = 2mm$. The calculated parameter of $R_f$, $w_s$, and $l_s$ , $h_f$ for ferrite circulator, are the initial design parameter with the possible need for optimizations after the structure of the circulator was modeled in order to get the best results at the center frequency of $2.4GHz$. Table 4.2 shows the design parameter of the ferrite circulator.

**Table 4.2: Design parameter of the ferrite circulator**

| Property | Values |
|---|---|
| Radius of Ferrite($R_f$) | $5.7mm$ |
| Ferrite Disk Thickness($h_f$) | $2mm$ |
| Width of the Stripline($w_s$) | $6mm$ |
| Length of the Stripline($l_s$) | $7mm$ |
| Thickness of the Stripline | $0.0035mm$ |

### Effect of radius of the ferrite ($R_f$)

Simulated responses by varying the radius of the ferrite ($R_f$) are summarized in Fig.4.5. Saturation magnetization ($M_s$) and Magnetization ($H_{in}$) are kept constant at 3200 $Gauss$ and 1000 $Oe$, respectively. The impedance matching for different $R_f$ are shown in Fig.4.5.(a), where the $S_{11} < -10\ dB$ for all considered values, but the lowest $S_{11}$ is observed with $R_f = 5.7$ mm. $S_{21} = -1.8dB$ is observed with this ferrite radius as shown in Fig.4.5.(b). The loss is dominantly due to the loss in the ferrite material and imperfect isolation. Significantly, low $S_{31}$ is observed in Fig.4.5.(c) indicates a good isolation from Port 1 to Port 3. From these investigations, it can be concluded that, the circulator offers good impedance matching, low insertion loss and isolation at $2.45GHz$ with $R_f = 5.7\ mm$.

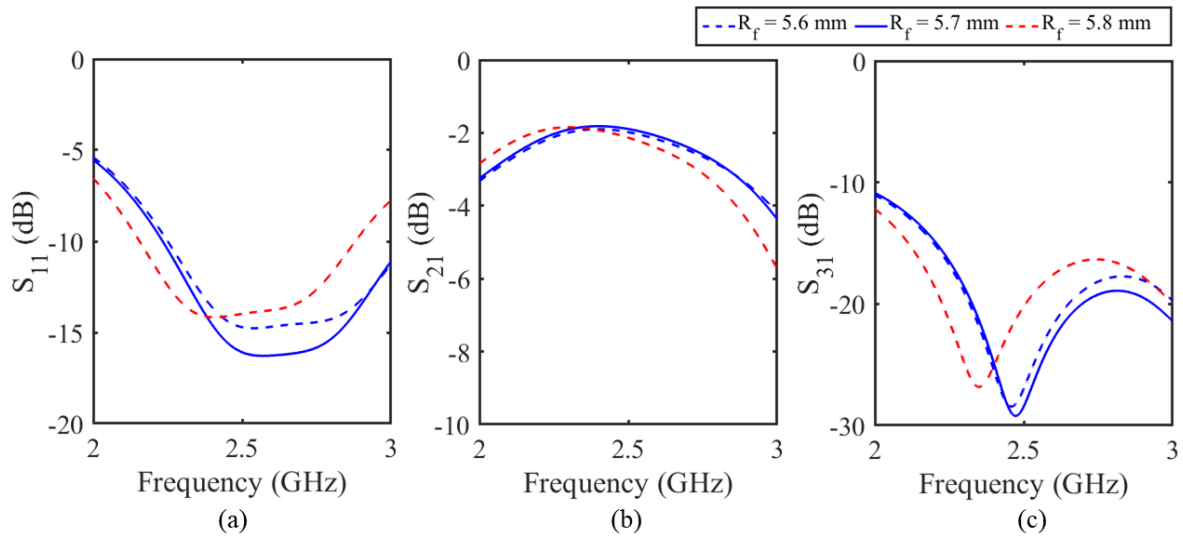


Fig.4.5: S-parameters of the Simulation for different values of ferrite radius (a) $S_{11}$, (b) $S_{21}$ and (c) $S_{31}$

**Effect of Saturation Magnetization ($M_s$)**

Simulated responses by varying the Saturation Magnetization ($M_s$) are summarized in Fig.4.6. Radius of the ferrite disc ($R_f$) and Magnetization ($H_{in}$) are kept constant at 5.7 mm and $1000\ Oe$ respectively. The input impedance matching at Port 1 improves with an increase in $M_s$ as shown in Fig.4.6.(a). Marginal variations are observed in the $S_{21}$ as approximately $-1.8dB$ of insertion loss is offered by the circulator at $2.45GHz$ as shown in Fig.4.6.(b). Significantly low $S_{31}$ are observed indicating good isolation from Port 1 to port 3 as shown in Fig.4.6.(c).

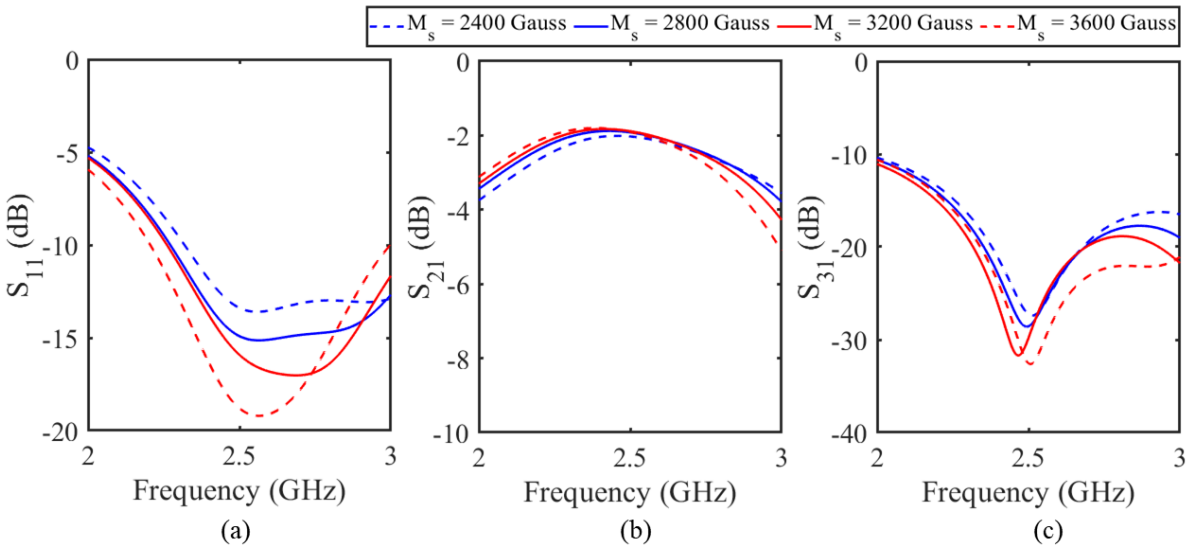


Fig.4.6: S-parameters of the Simulation for different Saturation Magnetization (a) $S_{11}$, (b) $S_{21}$ and (c) $S_{31}$

**Effect of Magnetization ($H_{in}$)**

Simulated responses by varying the Magnetization ($H_{in}$) are summarized in Fig.4.7. Radius of the ferrite disc ($R_f$) and Saturation Magnetization ($M_s$) are kept constant at $5.7mm$ and $3200Gauss$ respectively. The impedance matching at $2.45GHz$ improves by increasing $H_{in}$, and the lowest $S_{11}$ is observed for $H_{in} = 1000\ Oe$ as shown in Fig.4.7.(a). Similarly, the insertions loss response shifts to a higher frequency with $H_{in}$, and the $S_{21}$ is maximum at $2.45GHz$ with the same $H_{in}$ as shown in Fig.4.7.(b). The isolation at $2.45GHz$ is also significantly low with $H_{in} = 1000\ Oe$ as shown in Fig.4.7.(c).

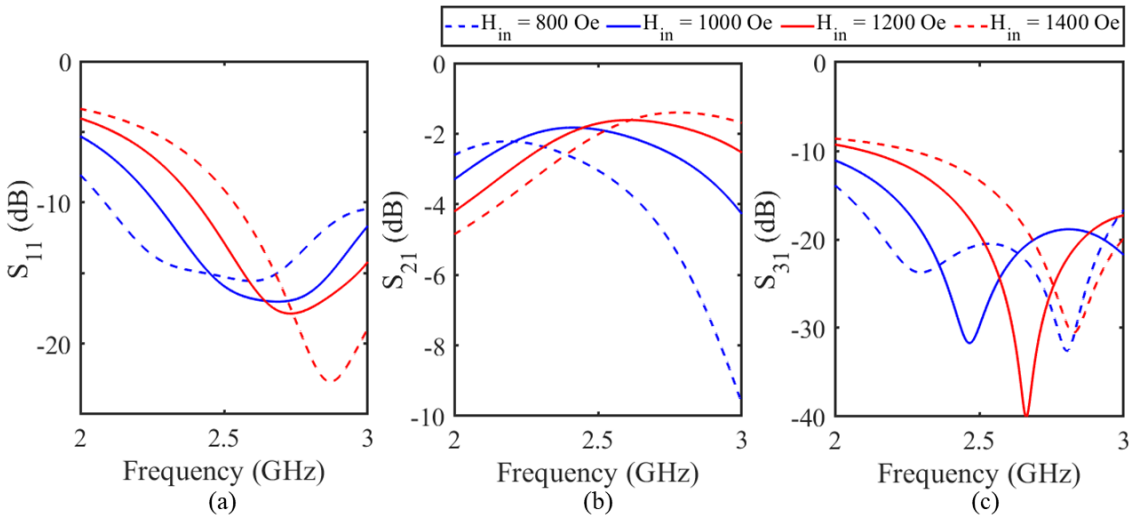


Fig.4.7: S-parameters of the simulation for different magnetization (a) $S_{11}$, (b) $S_{21}$ and (c) $S_{31}$

**Proposed geometry**

Considering the above investigation, $R_f = 5.7\,mm$, $M_s = 3200$ Gauss and $H_{in} = 1000$ Oe are selected for the proposed design. The simulated S-parameters are summarized in Fig.4.8 by exciting at all ports sequentially. Good impedance matching is observed at all the ports, and the matching ($S_{11}$, $S_{22}$ and $S_{33}$) is below $-10dB$ at $2.45GHz$. The $S_{21}$, $S_{32}$ and $S_{13}$ are approximately $-1.8dB$ indicating the flow of EM wave from Port 1 to port 3 through Port 2. But there is no power flow in the opposite direction as $S_{12}$, $S_{23}$ and $S_{31}$ are significantly low at the operating frequency as shown in Fig.4.8. The impedance matching, insertion loss and isolation responses from all ports overlap with each other which indicate an uniform flow of power in a single direction with an uniform circuit response between the ports.

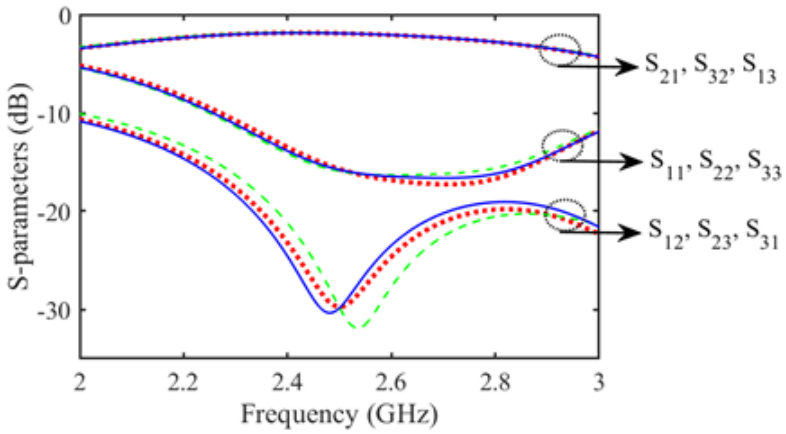


Fig.4.8: S-parameters of the optimized ferrite circulator

To visualize the unidirectional flow of fields in the designed circulator, the electric fields at $2.45GHz$ are plotted among the ports as shown in Fig.4.9. It can be observed that the field is concentrated between the desired ports without any coupling of power in the isolated ports.

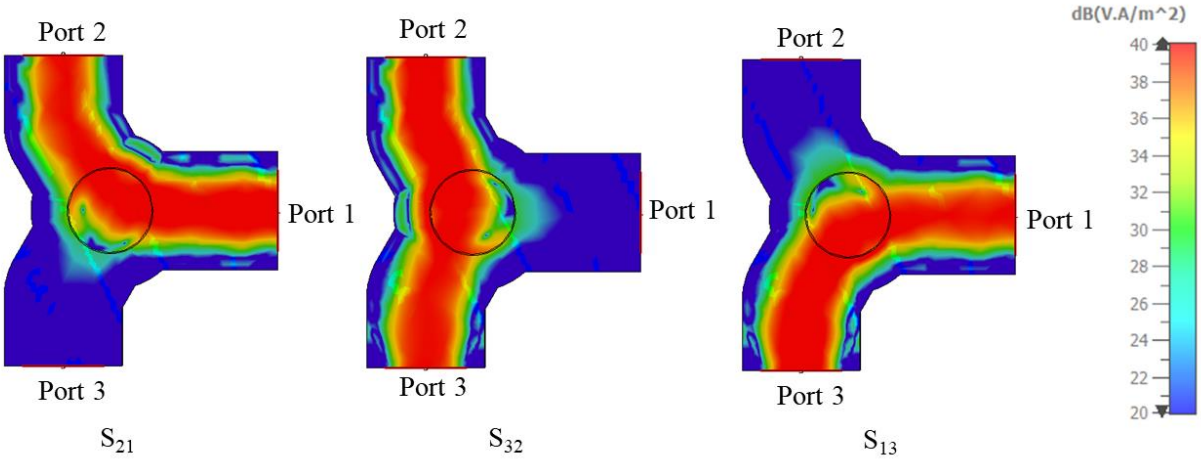


Fig.4.9: Direction of power flow considering port 1, 2 and 3 as input port respectively

## 4.3.2. Design of a ferrite less planar circulator

Planer circulators are investigated using couplers and different other designs are discussed in the literature. In [73], a simple ferrite less circulator design is proposed using an asymmetric power divider, and a couple of branch line coupler that can drive the power in a unidirectional way around the circuit as shown in Fig.4.10.

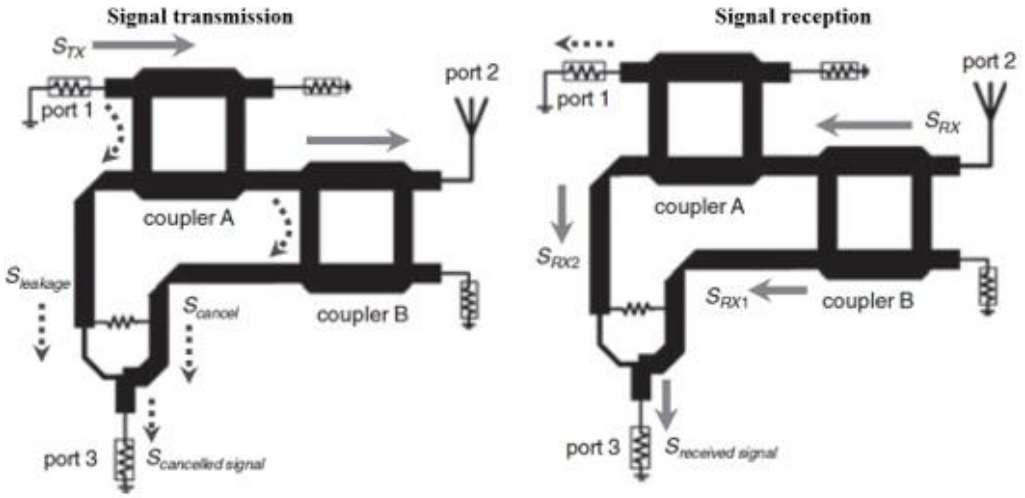


Fig.4.10: Schematic of a ferrite-less planar circulator showing the transmitting and receiving sides.

A part of the transmitting signal is coupled to the isolation ports of the branch-line couplers. The coupled signals at the isolation ports of coupler A and coupler B, $S_{leakage}$ and $S_{cancel}$ are $180^0$ out-of-phase with an amplitude difference of $3dB$. Therefore, to cancel out the leakage signals, an asymmetric power combiner are used whose output is denoted by port 3. These cancellations are as follows:

$$S_{leackage} = S_{TX} \times A_{leackage} \times e^{-j\theta leakage} \quad (4.6)$$

$$S_{cancle} = S_{TX} \times 0.5 \times e^{-j\pi} \times A_{leakage} \times e^{-j\theta leakage} \quad (4.7)$$

$$S_{cancelled\ signal} = 0.5 \times S_{leakage} + S_{cancel} \quad (4.8)$$

Where, $S_{TX}$ is the transmitting signal amplitude, $A_{leakage}$ is the ratio of the transmitting signal to the isolation port, and $\theta_{leakage}$ is the phase deviation. It demonstrated the isolation between port 1 and port 3, i.e. no power from port 1 is flowing to port 3.

The received signal from the antenna is split into two quadrature signals in the coupler where, one of the signal experiences an additional $90°$ phase delay and $3dB$ attenuation through coupler A. Since the two received signals of $S_{RX1}$and $S_{RX2}$ have the same phase and power difference of $3dB$, the output signal of the power divider/combiner ($S_{received}$) has a combined loss of $2dB$. The receiving process is as follows-

$$S_{RX1} = S_{RX} \times 0.5 \times e^{-j\pi} \quad (4.9)$$

$$S_{RX2} = S_{RX} \times (0.5 \times e^{-j\pi/2})^2 = S_{RX} \times 0.25 \times e^{-j\pi} \quad (4.10)$$

$$S_{received\ signal} = S_{RX1} + 0.5 \times S_{RX2} = 0.625 \times e^{-j\pi} \times S_{RX} \quad (4.11)$$

This approach is adopted in this thesis work to design a planar ferriteless circulator at 2.45 GHz.

**Branch line coupler**

A branch line coupler or $90°$ hybrid is a four-port network dividing the power between two ports equally with a $90°$ phase shift, isolating the other port from the input. The corresponding s-parameter is given as

$$[S] = -\frac{1}{\sqrt{2}}\begin{bmatrix} 0 & j & 1 & 0 \\ j & 0 & 0 & 1 \\ 1 & 0 & 0 & j \\ 0 & 1 & j & 0 \end{bmatrix}$$

A branch line coupler is designed in this section for 2.45 GHz.

**Schematic**

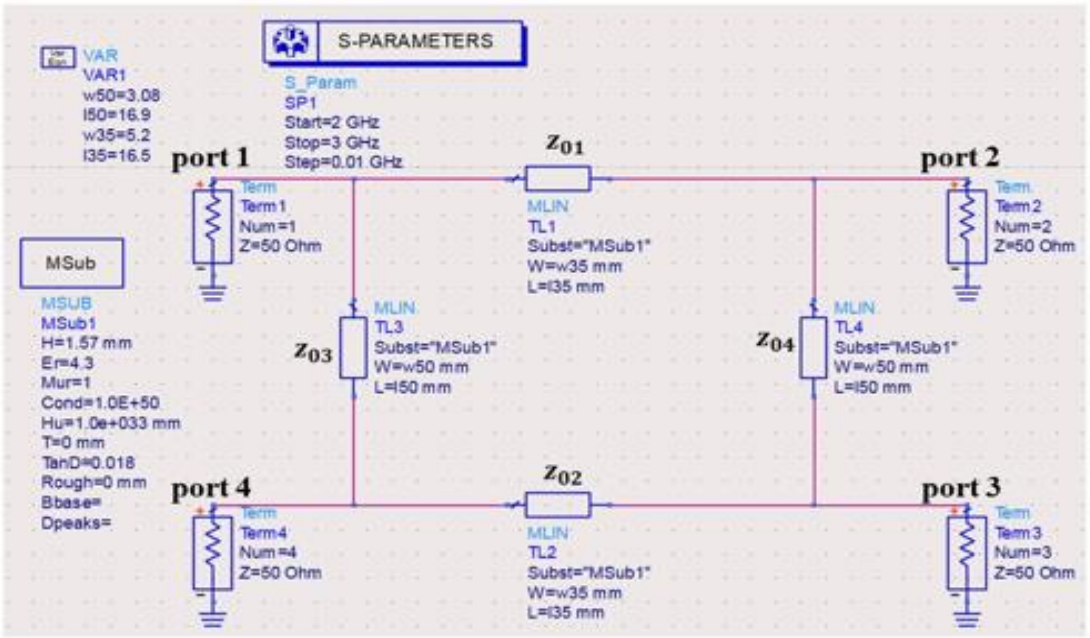


Fig.4.11: Simulated schematic of the branch line coupler

A branch line coupler is designed in ADS and the schematic is shown in Fig.4.11. Among the four ports, port 1 is the input port, port 2 is the direct port, port 3 is the coupled port and port 4 is the isolated port. Each arm of the coupler has a length of $\frac{\lambda}{4}$ ($\lambda$ is the guided wavelength at the operating frequency). The impedances of the two horizontal branches are $z_{01} = z_{02}\ z_0/\sqrt{2} =$ 35.5Ω and those for the vertical branches, it is $z_{03} = z_{04} = z_0$ = 50 Ω where, $z_0$ is the characteristics impedance of the lines. All ports are terminated with 50 Ω impedances.

An FR-4 substrate of thickness $1.57mm$ is considered to design the coupler using a microstrip configuration. Therefore, each line has a length of $16.5mm$ considering the dielectric properties. Width of the $35\Omega$ and $50\Omega$ lines are $5.2mm$ and $3.0mm$ respectively. Additional lines of $50\Omega$ are attached to connect the ports with the coupler. The lengths of the arms are slightly modified to optimize the performance of the coupler at the desired frequency.

**Simulated results**

The simulated results of the designed branch line coupler are shown in Fig.4.12. It is already mentioned that, port 1 is considered as the input terminal and hence, the $|S_{11}|$, $|S_{21}|$, $|S_{31}|$ and $|S_{41}|$ are plotted in the figure. The $|S_{11}| < -10\,dB$ at the operating frequency

of 2.45 $GHz$ indicates a good impedance matching at this port, i.e., all power fed to this terminal enters the coupler without any reflection. The power is equally divided between port 2 and port 3 as $|S_{21}| = |S_{31}| = -3.2dB$ at $2.45GHz$ are observed. Ideally, $3dB$ power should be delivered to the ports, but the dielectric loss resulted a reduction in the output powers. The $|S_{41}|$ is at the operating frequency is significantly low (approximately $-18dB$) that indicates a good isolation between port 1 and port 4. Hence, the designed branch line coupler is able to achieve the theoretically the predicted performance of dividing the input power equally between two powers by keeping the other port isolated.

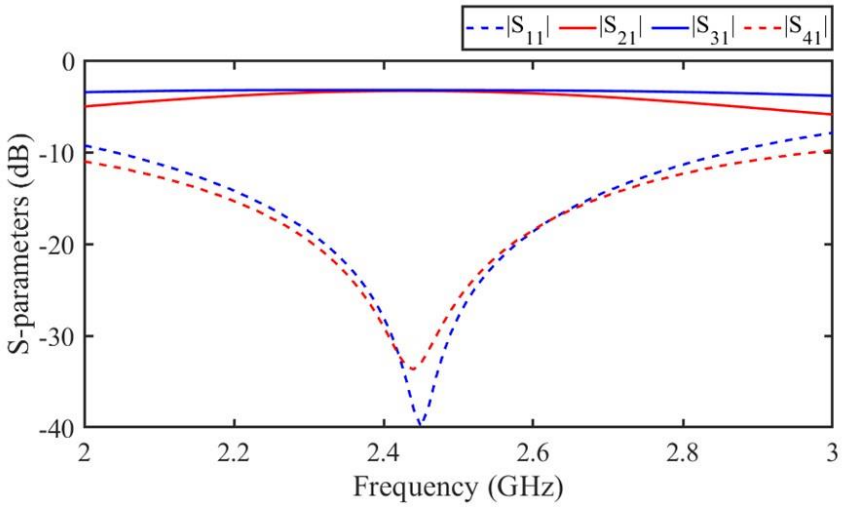


Fig.4.12: Simulated results of the branch line coupler

**Asymmetric power divider**

A power divider circuit is one that divides the input power among the desired number of ports. A simple three port network can be used as a power divider by modifying their arm impedances suitably. A Wilkinson power divider is a similar power divider circuit which is a three-port matched network with lossy element. But, a typical Wilkinson power divider divides the power equally between two arms which is not needed in our requirement. In our work, the input power is divided at a $1:2$ ratio between the output ports using an asymmetric power division (ASPD) circuit. The theory of unequal power division is well established and discussed in [74].

**Schematic of the ASPD Circuit**

Schematic of the ASPD circuit in ADS is shown in Fig.4.13. It is a three-port network where the input power at port 1 is divided among port 2 and port 3 by a factor of $1:2$. The

power divider network has two arms of length $\frac{\lambda}{4}$ of impedances of $z_{02}$ and $z_{03}$ with a lumped resistor of $R$ between the arms near the terminals. The impedance values are determined based on the power division ratio $p2:p3$ using the following formula:

$$K^2 = p3/p2 = 2$$

$$z_{03} = z_0\sqrt{\frac{1+K^2}{K^3}} = 103\ \Omega$$

$$z_{02} = K^2 z_{03} = z_0\sqrt{K(1+K^2)} = 51\ \Omega$$

$$R = z_0(K + \frac{1}{K}) = 106\ \Omega$$

But the impedances at port 2 and port 3 are not matched to 50 Ω and they are determined by:

$$z_{02-out} = z_0 K = 35\ \Omega$$

$$z_{03-out} = \frac{z_{03}}{K} = 71\ \Omega$$

To match the impedances at port 2 and port 3 with $50\Omega$, $\frac{\lambda}{4}$ lines of impedances $59\Omega$ and $42\Omega$, are used respectively.

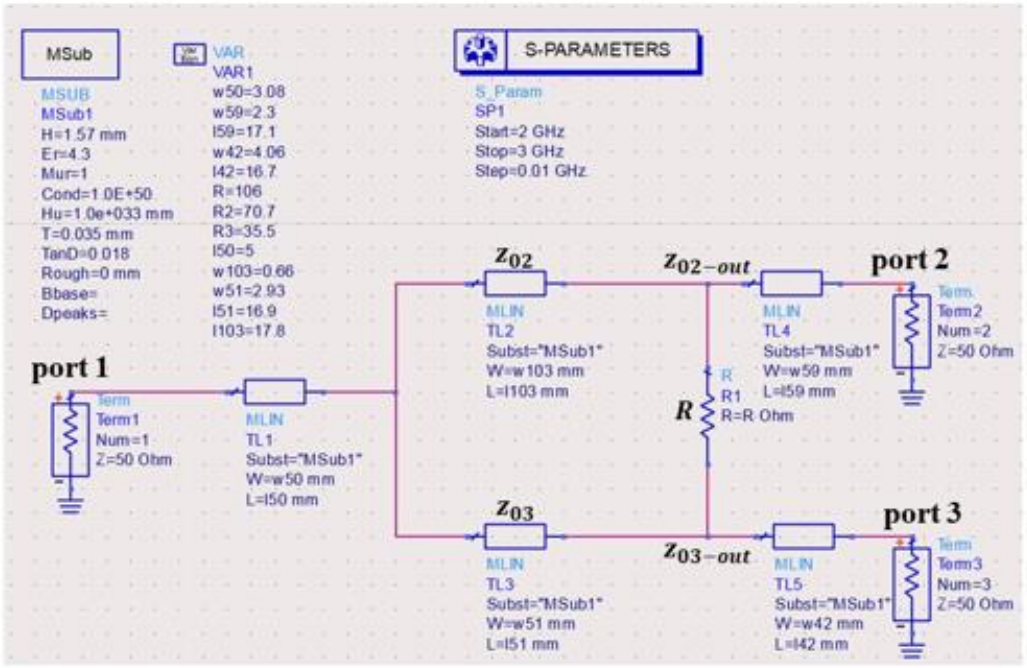


Fig.4.13: Simulated schematic of the asymmetric power divider

Considering the FR-4 dielectric of thickness 1.57mm, the $\frac{\lambda}{4}$ lines have lengths of approximately 17 mm. The lengths are marginally varied to optimize the results. Widths of the 103Ω, 51Ω, 59Ω and 42Ω lines are 0.66mm, 2.93mm, 2.3mm and 4.026mm, respectively. The schematic shown in Fig. is simulated to validate its responses.

**Simulated Results**

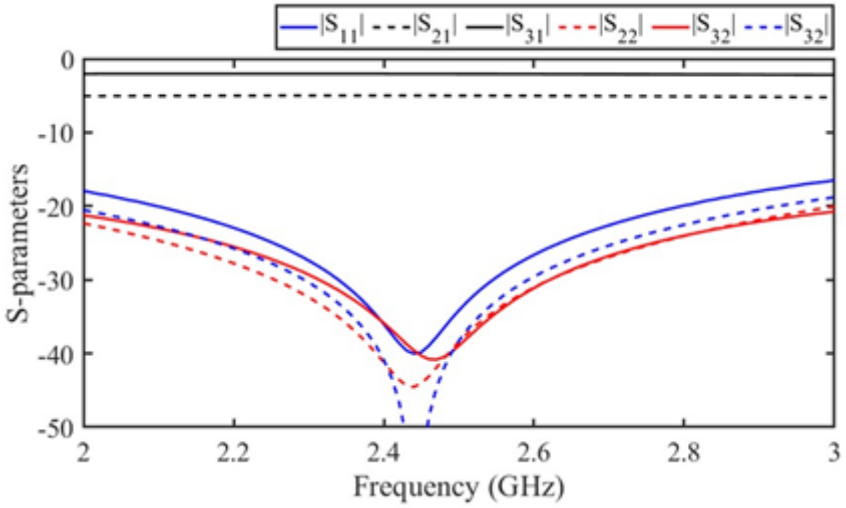


Fig.4.14: Simulated results of the ASPD

The simulated $S_{11}$ is significantly below $-10dB$ indicating a good impedance matching at the input. Also, $|S_{21}| = -6.2dB$ and $|S_{31}| = -2.1dB$ are observed, i.e., the power delivered to port 2 is half of that of port 3 meeting the required power ratio at the ports. The reduction in the power levels are due to the dielectric loss of the substrate. The power fed to port 2 and port 3 enters the network without reflection at the ports as significantly low $S_{22}$ and $S_{33}$ are observed. But these two ports are isolated as $S_{32}$ is approximately $-50dB$ at the operating frequency. Hence, an asymmetric power divider is designed meeting the desires criteria required to design the ferrite less circulator.

**Schematic of the ferrite less planar circulator**

Schematic of the ferrite less planar circulator consisting of two branch line couplers and one ASDP are shown in Fig.4.15. The input of the circulator is fed at the port 1 of BLC 1. The port 2 of BLC 1 is terminated with a matched load and port 3 to the input of BLC 2. Port 3 of BLC 3 is terminated with a matched load and the port 2 is used as the second port of the circulator. Port 4 of BLC 1 and BLC 2 are connected to the port 2 and port 3 of the ASPD, respectively. The port 2 of ASPD is considered as the port 3 of the circulator.

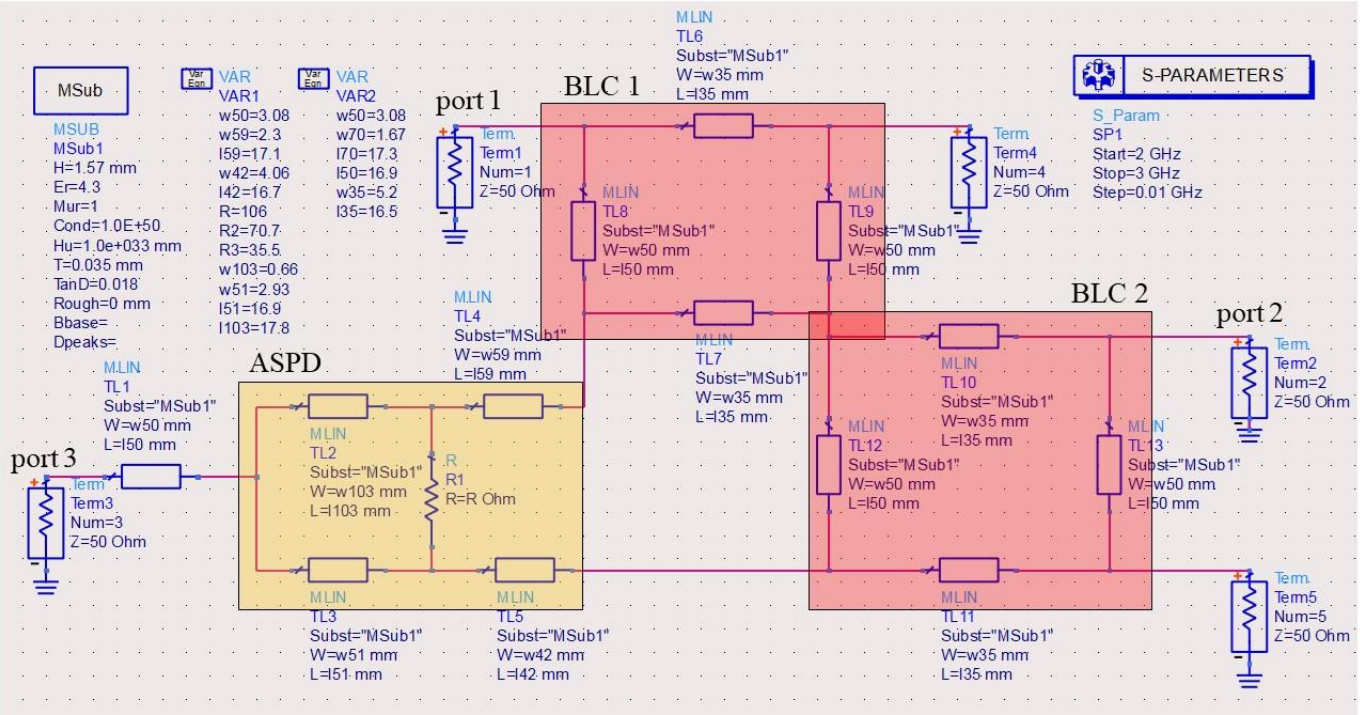


Fig.4.15: Schematic of the proposed ferrite less planar circulator

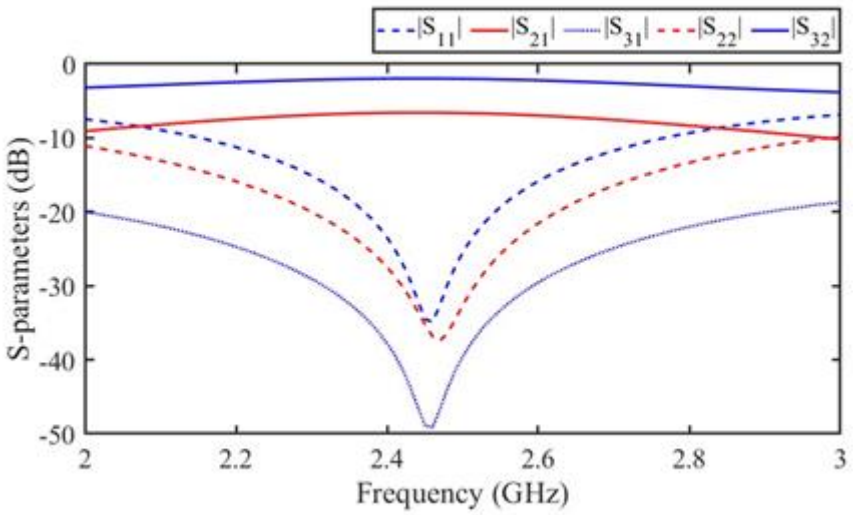


Fig.4.16: Simulated results of the circulator

**Simulated Results**

The circulator geometry is simulated in ADS using the s-parameter simulation machine between $2GHz$ to 3GHz. The power fed to port 1 enters the circuit without reflections as $|S_{11}| < -10dB$ at 2.45GHz. The power is transferred to port 2 as $|S_{21}|$ is approximately$-6dB$. But no power from port 1 is guided towards port 3 as $S_{31}$ is significantly low. The $S_{22}$ is below $-10dB$ indicating a good impedance matching at this

port. The power fed to port 2 is guided to port 3 as $S_{32} = -2dB$ is observed at the frequency of operation. Hence, the power at port 1 travels to port 2 and that at port 2 travels to port 3 without any reflection. The losses are due to the circulator configuration and due to the dielectric losses of the substrate. Therefore, a ferrite less planer circulator is designed to work at the junction of a transceiver circuit. The transmitter is connected to the port 1 and the receiver is at port 3. The antenna is connected at port 2 that communicates with both sections without any coupling between them. The power losses in the circuit can be avoided by modifying the circulator design which is a left as a future work.

## 4.4. Proposed Smart Tracking and Beam Steering technique

### 4.4.1. Receiving Chain

Block diagram of the receiving chain is shown in Fig.4.17. The $1 \times 8$ antenna array in the base station receives the RF power from the user. The received RF power is isolated from the transmit chain using a circulator which is connected to the antenna output. The received RF is converted to equivalent DC voltage by using a rectenna circuit which is fed to the 'maximum power detection logic' block. This block consisting of a magnitude comparator circuit followed by a decision-making boolean logic circuit. It compares the DC levels from the seven other RF chains and generates the index of the antenna receiving the maximum RF power. This index is fed to the phase generator circuit that generates the desired phase to steer the antenna main beam towards the user.

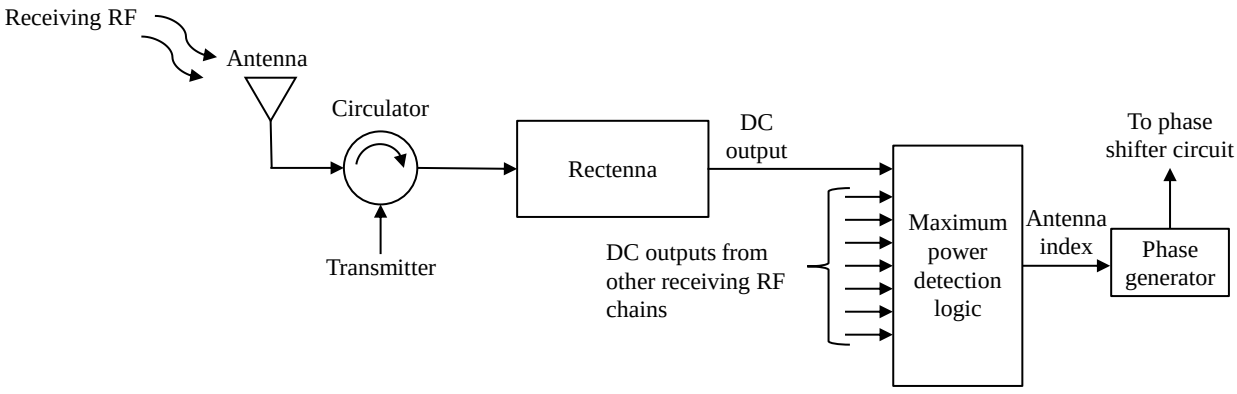


Fig.4.17: Block Diagram of Receiving chain

### 4.4.2. Transmitting Chain

After the user location is determined, the antenna main beam is steered towards the desired direction and the RF is power is radiated. Block diagram of the designed transmit chain is shown in Fig.4.18. The continuous RF signal is fed to the power divider circuit that

divides the power among eight equal channels. The RF power is fed to the phase shifter circuit where the shifting is determined by the output of decision making circuit in the receiving chains. The phase shifted RF signal is fed to the antenna through the circulator that isolates the receiving section of the receiver.

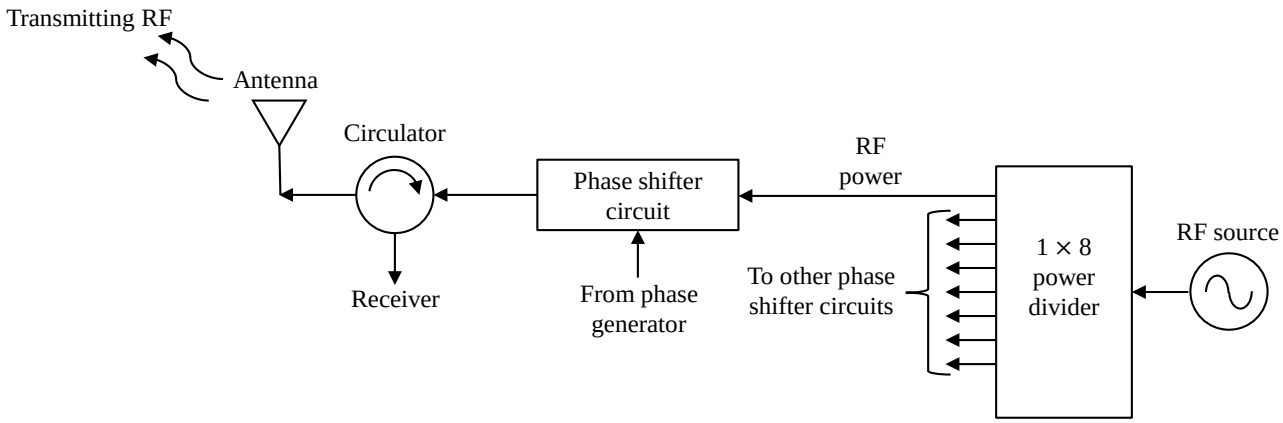


Fig.4.18: Block Diagram of Transmitting Chain

### 4.4.3. Transceiver chain

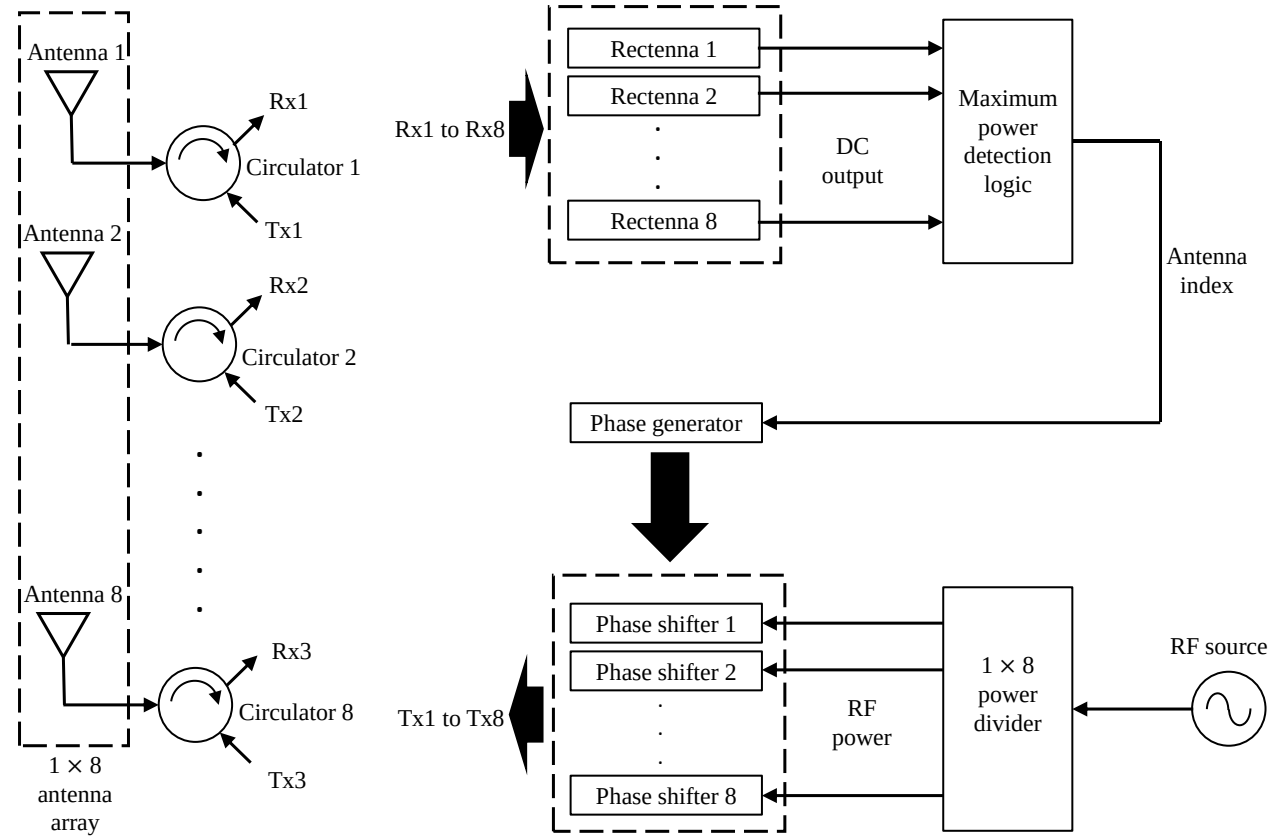


Fig.4.19: Block Diagram of the Smart Tracking System

The Block diagram of the proposed smart tracking and beam steering system by concatenating the transmitting and receiving system together is shown in Fig. 4.19. The $1 \times 8$ antenna array receives the RF from the user location which are fed to the receiving chain through the bank of eight circulators. The eight DC outputs generated by the set of rectenna circuit are processed in the comparator circuit to generate the index of the antenna receiving the maximum RF power. The index is fed to a phase generator that generates the desired phase for beam steering. At the transmitter section, the input RF is divided into eight equal parts whose phase is tuned by the phase shift circuit. The phase shifted RF signal is fed to the antenna array through the circulator. Based on the relative phase of the antenna inputs, the overall antenna beam is steered toward the user location to utilize the antenna radiation effectively.

## 4.5. Summary

In 4.2.1, the concept of user location detection using the received signal amplitude is presented. The relative locations in the lateral as well as longitudinal directions are determined by the received RF of the antenna array. In 4.3 designs of circulators as a decoupling circuit between the transmitting and receiving RF chains are presented. Design of a conventional ferrite based circulator is investigated which is followed by the design of a ferrite less planer circulator geometry consisting of a pair of branch line coupler and an asymmetric Wilkinson power divider. The former has a better isolation whereas the later has a compact and planar geometry. In 4.4 the transmit, receive and complete RF chain of the proposed smart tracking and beam steering technique were presented using the respective Block Diagrams, and their operations are briefly explained.

# CHAPTER 5

# Conclusion and Future work

## 5.1. Conclusion

In this Thesis work, a smart tracking based beam steering technique is investigated to utilize the maximum radiation of a base station to track a moving target / user. An extensive literature review is carried out to build the theoretical background and for proper comparative study in order to improve the performance of the proposed system. The proposed system consists of a receiving chain for tracking and a transmit chain for steering operation. The user location is accurately determined in the tracking system using DC level magnitude comparison instead of RF signals that simplifies the overall circuit. To understand the working of this approach, the location of a dipole antenna (user) about a patch antenna array is varied, and the variation in the received magnitudes is analyzed numerically.

A miniaturized microstrip patch antenna is designed to transmit and receive the RF signals in the transceiver chain. An asymmetric slot is used to miniaturize the patch antenna for 2.45 $GHz$ with 23% area of a reference radiator. Parametric investigations are carried out to optimize the antenna geometry and to understand the miniaturization procedure. An $1 \times 8$

array of the proposed antenna is designed to obtain a narrow beam and a high gain radiating aperture to facilitate the beam steering operation. A corporate feed network is designed to energize the antenna array using a single RF source. The feed network includes a simple and lossless power division network that equally divides the input power among the antennas. A phase shifter circuit is also embedded in the feeding network to inspect the steering operation by varying the input phases. Using a dual-layer board consisting of the antenna array and a feed network on opposite sides of the substrate separated by the ground plane is designed, and approximately $\pm 22^0$ of phase shift is observed over the azimuthal plane.

In the receiving chain, a magnitude based smart tracking system is investigated that consists of a rectenna, a magnitude comparator and a digital logic system. Since the user's location closest to an antenna element of the array will receive the maximum RF signal power, the antenna outputs are processed to determine the user location accurately. A diode-based rectenna is designed to convert the received RF by the antennas into equivalent DC outputs. It is optimized for the load resistor as well as for input power observing a maximum of approximately $42\%$ conversion efficiency. Using numerical analysis, it is also shown that the designed circuit can convert the RF power from the fundamental harmonic ($2.45\ GHz$) into the DC or $0^{th}$ harmonic, effectively. But these DC voltages have an analogue variation in their amplitudes which makes the decision-making circuitry (tracking angle) complex. Therefore, these amplitudes are mapped into digital signals using an op-amp based magnitude comparator circuit. This circuit referred to as DC level comparison compares all the DC outputs, and generated a set of digital signals. These digital outputs are fed into a Boolean logic circuit that generates the antenna index receiving the maximum RF power. The comparator, as well as the digital circuit, is numerically investigated to demonstrate the working of the proposed tracking system. The index is used to drive a phase shifter circuit to steer the antenna main beam in the desired direction.

The transmit and receive chains are connected to the antenna network through a decoupling circuit that maintains the unidirectional flow of EM power in the transceiver isolating the chains from each other. A ferrite based simple circulator circuit is designed to work at $2.45GHz$ and has good impedance matching with an insertion loss of $-1.8dB$. Moreover, it provides excellent isolation between the desired ports allowing a unidirectional power flow as required. But the presence of ferrite makes the geometry non-planar and bulky. Therefore, a planar circulator consisting of a pair of branch-line couplers and an asymmetric Wilkinson power divider is designed for this purpose. Using analytical and numerical

investigations, it is shown that the circuit can facilitate a unidirectional flow of EM power with good impedance matching. But, degraded isolation is observed between the desired ports with a high insertion loss in this circuit. Further, the transmitter and receiver chains are described by stitching the individual working blocks together. Finally, the working of the proposed beam steering technique based smart tracking system is explained with the complete block diagram.

## 5.2. Broad Application Areas of the Proposed Scheme:

The proposed system can be potentially used for

- Cellular networks to provide an uninterrupted communication by tracking the user in the 2D plane along the elevation in a cell-based mobile system.
- Driverless car or for unmanned aerial vehicle (UAV) to track the relative location of neighbouring objects.
- Different radar applications to detect the movement of aircrafts from an air traffic control system.
- Doppler imaging for weather radar applications.
- High frequency in $5G$ (around $28\ GHz$) and high frequency WiFi ($77\ GHz$) for indoor applications.

## 5.3. Future work

Despite the effectiveness of the proposed approach, the following aspects can be improved and may be considered as a part of the future work:

- The antenna uses an asymmetric patch to increase the current path along a U-shaped path. This may reduce the radiation efficiency of the antenna leading to a degraded antenna gain. Hence, the proposed miniaturization technique may be modified to overcome this issue.
- The antenna array can provide a maximum of $\pm 22$ degree of steering over the azimuthal direction. The antenna geometry and the feeding network can be modified to tilt the antenna radiation at a higher angle.
- The phase shift operation is implemented by varying the path length at the antenna inputs. Digital phase shifter ICs can be used on the RF traces to facilitate continuous steering of the main beam.

- The efficiency of the rectenna circuit can be improved by using another diode or a different matching network.
- Since the outputs of rectenna are practically very small, an amplifier or level shifter circuit may be employed before the magnitude comparator stage.
- The insertion loss and isolation in the circulators can be improved by modifying the ferrite or the passive circuit elements properly.
- An FR-4 dielectric is considered for all investigations which resulted in higher insertion loss due to a higher loss tangent.
- The fabrication and experimental validation are required to demonstrate the usefulness of the proposed tracking system.

## 5.4. Publication

The findings of this Thesis work has been presented at the 2022 IEEE International Conference on Signal Processing and Communication (IEEE SPCOM 2022) held at IISc Bangalore as per the details given below:

Paramita Saha, Jagabandhu Das, P. Venkateswaran, "Smart Beam Steering with a Slot-Loaded Miniaturized Patch Antenna," 2022 IEEE International Conference on Signal Processing and Communications (SPCOM), Indian Institute of Science, Bangalore, July 11-15, 2022.

The author has presented the paper on July 15, 2022 on virtual platform.

# REFERENCES


[1] D. Bonefacic and J. Jancula, "Laboratory Model of a Monopulse Radar Tracking System," *Proceedings ELMAR 2006*, 2006, pp. 227-230.

[2] S. Gogineni and A. Nehorai, "Target tracking using monopulse MIMO radar with distributed antennas," *2010 IEEE Radar Conference*, 2010, pp. 194-199.

[3] S. Gogineni and A. Nehorai, "Monopulse MIMO Radar for Target Tracking," in *IEEE Transactions on Aerospace and Electronic Systems*, vol. 47, no. 1, pp. 755-768, January 2011.

[4] G. M. Brooker, "Conical-scan antennas for W-band radar systems," *2003 Proceedings of the International Conference on Radar (IEEE Cat. No.03EX695)*, 2003, pp. 406-411.

[5] R. C. Eggleton and K. W. Johnston, "Real Time Mechanical Scanning System Compared with Array Techniques," *1974 Ultrasonics Symposium*, 1974, pp. 16-18.

[6] S. Sumeem, S. A. Ahmed and S. A. Khan, "System on reconfigurable chip for automatic detection and tracking radar," *8th International Multitopic Conference, 2004. Proceedings of INMIC 2004.*, 2004, pp. 146-151.

[7] G. L. Bair and E. D. Zink, "Radar track-while-scan methodologies," *IEEE Region 5 Conference, 1988: 'Spanning the Peaks of Electrotechnology'*, 1988, pp. 32-37.

[8] R. J. Evans, C. R. Hewett and F. Barker, "Radar System Design for Track-While-Scan," *IEEE Transactions on Aerospace and Electronic Systems*, vol. AES-15, no. 1, pp. 125-133, Jan. 1979.

[9] L. Zhu, W. Su, S. Wu, Y. Wang and X. Shan, "Phased-Array Radar Beam Tracking and Predicting," *2009 5th International Conference on Wireless Communications, Networking and Mobile Computing*, 2009, pp. 1-4.

[10] G. van Keuk and S. S. Blackman, "On phased-array radar tracking and parameter control," *IEEE Transactions on Aerospace and Electronic Systems*, vol. 29, no. 1, pp. 186-194, Jan. 1993.

[11] Muhammad Irshad Khan , Muhammad Anab, Muhammad Kabir Khan, Saeed-Ur-Rahman and Aamir Sultan, “A Survey on Beam Steering Techniques in Printed Antennas,” International Journal of Recent Contributions from Engineering, Science and IT, vol. 9, no. 2, 2021.

[13] Carl B. Dietrich, Jr., “Adaptive Arrays and Diversity Antenna Configurations for Handheld Wireless Communication Terminals,” Doctor of Philosophy, Electrical and Computer Engineering, Virginia Polytechnic Institute and State University, Blacksburg, Virginia, February 15, 2000.

[14] A. Dhami, N. N. Parekh and Y. Vasavada, "Digital Beamforming for Antenna Arrays," 2019 IEEE Indian Conference on Antennas and Propogation (InCAP), 2019, pp. 1-5.

[15] M. I. Abbasi, M. H. Dahri, M. H. Jamaluddin, N. Seman, M. R. Kamarudin and N. H. Sulaiman, "Millimeter wave beam steering reflectarray antenna based on mechanical rotation of array," *IEEE Access*, vol. 7, pp. 145685-145691, 2019.

[16] Divaydeep Sikri and Rajanik Mark Jayasuriya, "Multi-Beam Phased Array with Full Digital Beamforming for SATCOM and 5G," *Microwave Journal*, April 11, 2019.

[17] S. Shahsavari, S. A. Hosseini, C. Ng and E. Erkip, "Adaptive Hybrid Beamforming with Massive Phased Arrays in Macro-Cellular Networks," *2018 IEEE 5G World Forum (5GWF)*, 2018, pp. 221-226.

[18] X. Liu, E. Wang and Z. Yan, "Dual-band Reflect-Transmit-Array Antenna with High-Gain and Low- Profile," *2021 IEEE International Symposium on Antennas and Propagation and USNC-URSI Radio Science Meeting (APS/URSI)*, 2021, pp. 1771-1772.

[19] A. Ghasemi, S. N. Burokur, A. Dhouibi and A. de Lustrac, "Phase-gradient metasurfaces for beam steerable antennas," *2014 International Workshop on Antenna Technology: Small Antennas, Novel EM Structures and Materials, and Applications (iWAT)*, 2014, pp. 191-194.

[20] M. J. M. van der Vorst, P. J. I. de Maagt and M. H. A. J. Herben, "Scan-Optimized Integrated Lens Antennas," *1997 27th European Microwave Conference*, 1997, pp. 605-610.

[21] S. K. Karki, J. Ala-Laurinaho, A. Kantunen and V. Viikari, "Integrated Lens Antennas for E-Band," *2018 48th European Microwave Conference (EuMC)*, 2018, pp. 1151-1154.

[22] Ruchi Agarwal, Prakhar Pratap Singh, Suresh Kumar, Umang Singh, Vipul Agarwal, "Leaky Wave Antenna for Wide Angle Beam Scanning and High Directivity," *Advances in Smart Communication and Imaging Systems, Select Proceedings of MedCom 2020*, April 2021.

[23] Solomon MingleIhab, HassounIhab Hassoun, Walid Kamali ,"Beam-Steering in Metamaterials Enhancing Gain of Patch Array Antenna Using Phase Shifters for 5G Application," *IEEE EUROCON 2019 -18th International Conference on Smart Technologies*, July 2019.

[24] Ankit Singh, Ankit Kumar, Abhishek Ranjan, Arvind Kumar, Arun Kumar, "Beam Steering in Antenna," *International Conference on Innovations in information Embedded and Communication Systems (ICIIECS)*, 2017.

[25] N. Hasegawa,Y. Takagi,Y. Nakamoto and Y. Ohta, "2-D Beam Steering by the Simple Phased-Array Technique for Microwave Power Transfer," *2020 IEEE Asia-Pacific Microwave Conference (APMC)*, 2020, pp. 185-186.

[26] A. Kurt and M. S. Boybay, "A Novel Low-Cost Beam Steering Method Using Dispersive Superstrate," *2018 IEEE International Symposium on Antennas and Propagation & USNC/URSI National Radio Science Meeting*, 2018, pp. 2547-2548.

[27] Iyemeh Uchendu and James R. Kelly," Survey of Beam Steering Techniques Available for Millimeter Wave Applications," *Progress In Electromagnetics Research B*, Vol. 68, 35-54, 2016.

[28] A. Singh, A. Kumar, A. Ranjan, A. Kumar and A. Kumar, "Beam steering in antenna," *2017 International Conference on Innovations in Information, Embedded and Communication Systems (ICIIECS)*, 2017, pp. 1-4.

[29] T. Kushwaha, D. K. Singh, "A Review on Beam Steering Techniques in Reconfigurable Microstrip Patch Antennas," *International Journal of Advanced Research in Computer Engineering & Technology (IJARCET)*, Vol. 6, Issue 9, Sep. 2017.

[30] I. E. Uchendu, J. R. Kelly, R. Mittra and Y. Gao, “Hybrid Parasitic Linear Array Antenna for Fine Beam steering Applications,” *IEEE Access*, vol. 9, pp. 84899-84909, 2021.

[31] C. A. Balanis,“Antenna Theory: Analysis and Design,” *Wiley-India*, 2nd ed., 2009.

[32] A. A. Rakholiya, N. V. Langhnoja, “A review on miniaturization techniques for microstrip patch antenna,” *International Journal of Advance Research and Innovative Ideas in Education (IJARIIE)*, vol. 3, issue 2, 2017.

[33] D. Schaubert and K. Yngvesson, ”Experimental study of a microstrip array on high permittivity substrate,” *IEEE Transactions on Antennas and Propagation*, vol. 34, no. 1, pp. 92-97, January 1986.

[34] S. I. Hussain Shah, S. Bashir and A. Altaf, ”Miniaturization of microstrip patch antenna by using various shaped slots for wireless communication systems,” *2014 XIXth International Seminar/Workshop on Direct and Inverse Problems of Electromagnetic and Acoustic Wave Theory (DIPED)*, 2014, pp. 92-95.

[35] T. K. Upadhyaya, V. V. Dwivedi, S. P. Kosta and Y. P. Kosta, ”Miniaturization of Tri Band Patch Antenna Using Metamaterials,” *2012 Fourth International Conference on Computational Intelligence and Communication Networks*, 2012, pp. 45-48.

[36] D. De, A. Prakash, N. Chattoraj, P. K. Sahu and A. Verma, "Design and analysis of various Wilkinson Power Divider Networks for L band applications," *2016 3rd International Conference on Signal Processing and Integrated Networks (SPIN)*, 2016, pp. 67-72.

[37] Z. -Y. Zong, J. -Q. Lu, J. Yang and B. Li, "Research on 3-dB wilkinson power divider with arbitrary phase-shift," *2015 Asia-Pacific Microwave Conference (APMC)*, 2015,pp. 1-3.

[38] J. Shi, J. Qiang, K. Xu, W. Qin, L. Zhou and Q. Cao, "A differential branch-line coupler," *2015 IEEE 4th Asia-Pacific Conference on Antennas and Propagation (APCAP)*, 2015, pp. 431-432.

[39] N. H. A. Rahim, R. Rasid, S. Z. Ibrahim, N. Khalid, M. S. Razalli and T. G. Siang, "Development of branchline coupler using parallel coupled transmission lines," *2016 3rd International Conference on Electronic Design (ICED)*, 2016, pp. 76-79.

[40] Jacho Chung, Byungje Lee and Mynn-Joo Park, "Branch line coupler with cross coupling," *34th European Microwave Conference*, 2004, pp. 285-288.

[41] T. Moyra, A. Roy, S. K. Parui and S. Das, "Design of 10 dB branch line coupler by using DGS," *2012 International Conference on Communications, Devices and Intelligent Systems (CODIS)*, 2012, pp. 516-519.

[42] H. Xu, G. Wang and K. Lu, "Microstrip Rat-Race Couplers," *IEEE Microwave Magazine*, vol. 12, no. 4, pp. 117-129, June 2011.

[43] B. Arigong, J. Shao, M. Zhou, J. Ding, H. S. Kim and H. Zhang, "A novel dual-band rat-race coupler," *WAMICON 2014*, 2014, pp. 1-3.

[44] C.Wu, Y.Chiou and J.Kuo, "Dual-band rat-race coupler with arbitrary power divisions using microwave C-sections," *2009 Asia Pacific Microwave Conference*, 2009, pp. 2108-2111.

[45] P.Tu and C.Tseng,"Design of a compact rat-race coupler using dual transmission lines," *2010 Asia-Pacific Microwave Conference*, 2010, pp. 1224-1227.

[46] R. L. Timsina, R. A. Messner and J. L. Kubwimana, "A compact design of switched line phase shifter for a microstrip phased array antenna," *2017 Progress in Electromagnetics Research Symposium - Fall (PIERS - FALL)*, 2017, pp. 1839-1844.

[47] Yulin Huang, Jingfu Bao, Xinyi Li, Yiling Wang and Yijia Du, "A 4-bit switched-line phase shifter based on MEMS switches," *10th IEEE International Conference on Nano/Micro Engineered and Molecular Systems*, 2015, pp. 405-408.

[48] I. Gharbi, R. Barrak, M. Latrach, H. Ragad and M. Menif, "Design of a switched line phase shifter for reconfigurable mm-wave Antennas," *2019 15th International Wireless Communications & Mobile Computing Conference (IWCMC)*, 2019, pp. 1440-1444.

[49] J. Zhang, S. W. Cheung and Q. Zhu, "Design of 180°-switched-line phase shifter with constant phase shift using CRLH TL," *2014 IEEE Antennas and Propagation Society International Symposium (APSURSI)*, 2014, pp. 344-345.

[50] I. Hussain, A. K. Rashid and H. Ullah, "Hybrid type of broad-band microwave phase shifter using schiffman lines," *Proceedings of 2013 10th International Bhurban Conference on Applied Sciences & Technology (IBCAST)*, 2013, pp. 381-384.

[51] R. -C. Han, R. -Y. Sun and S. -H. Shi, "A wideband planar hybrid coupler using coupled-line power divider and broadband phase shifter," *2017 Sixth Asia-Pacific Conference on Antennas and Propagation (APCAP)*, 2017, pp. 1-3.

[52] R. Sun, Q. Chen, R. Han and Z. Lu, "Analysis and Design of Wideband 90° Microstrip Hybrid Coupler," IEEE Access, vol. 7, pp. 186409-186416, 2019.

[53] K. -W. Han, H. Cui, X. -W. Sun and J. Zhang, "The design of a 60 GHz low loss hybrid phase shifter with 360 degree phase shift," *2014 14th International Symposium on Communications and Information Technologies (ISCIT)*, 2014, pp. 551-554.

[54] O. H. Karabey, F. Goelden, A. Gaebler, S. Strunck and R. Jakoby, "Tunable loaded line phase shifters for microwave applications," *2011 IEEE MTT-S International Microwave Symposium*, 2011, pp. 1-4.

[55] A. J. F. Orlando and B. Chambers, "Periodically Loaded Ferrite Phase Shifters," 1975 *5th European Microwave Conference*, 1975, pp. 508-512.

[56] M. M. Z. Kharadly, "Periodically Loaded Nonreciprocal Transmission Lines for Phase-Shifter Applications," IEEE Transactions on Microwave Theory and Techniques, vol. 22, no. 6, pp. 635-640, Jun. 1974.

[57] E. Wang, X. Fu and Q. Tian,"Broadband power divider with phase shifter," *2012 2nd International Conference on Consumer Electronics, Communications and Networks (CECNet)*, 2012, pp. 1700-1702.

[58] B. Dwivedy and S. K. Behera, "Design of a wideband equal power divider and multiple phase shifter for variable polarization," *2016 IEEE Students' Conference on Electrical, Electronics and Computer Science (SCEECS)*, 2016, pp. 1-5.

[59] Y. -P. Lyu, L. Zhu and C. -H. Cheng, "An Integration Perspective for Power Divider and Phase Shifter with Performance Enhancement : (Invited Paper)," *2020 IEEE Asia-Pacific Microwave Conference (APMC)*, 2020, pp. 383-385.

[60] B. A. Auld, "The Synthesis of Symmetrical Waveguide Circulators," IRE Transactions on Microwave Theory and Techniques, vol. 7, no. 2, pp. 238-246, April 1959.

[61] C. E. Fay and R. L. Comstock, "Operation of the Ferrite Junction Circulator," IEEE Transactions on Microwave Theory and Techniques, vol. 13, no. 1, pp. 15-27, January 1965.

[62] L. Marzall, D. Psychogiou and Z. Popović, "Microstrip Ferrite Circulator Design With Control of Magnetization Distribution," IEEE Transactions on Microwave Theory and Techniques, vol. 69, no. 2, pp. 1217-1226, Feb. 2021.

[63] W. M. Gitzel, S. Bahadori Rad, M. Heidenreich, J. Töpfer and A. F. Jacob, "Integration Concept for a Self-Biased Ka-Band Circulator," *2020 23rd International Microwave and Radar Conference (MIKON), 2020*, pp. 350-352.

[64] V.Kelaiya and M. R. Naik, "Design and simulation of X Band microstrip circulator," *2016 IEEE Region 10 Conference (TENCON)*, 2016, pp. 1961-1964.

[65] S. K. Jain and P. Pradeepkumar, "Design of Broadband Waveguide Circulator at Ka-Band," *2021 IEEE MTT-S International Microwave and RF Conference (IMARC)*, 2021, pp. 1-4.

[66] S.Hosszú, L.Jakab and T.Berceli,"Computer aided microstrip circulator design,"*18-th International Conference on Microwaves, Radar and Wireless Communications*, 2010, pp.1-4.

[67] E.J. Denlinger, "Design of Partial Height Ferrite Waveguide Circulators (Short Papers)," IEEE Transactions on Microwave Theory and Techniques, vol. 22, no. 8, pp. 810-813, Aug. 1974.

[68] Okba A, Takacs A, Aubert H, Charlot S, Calmon P-F. Multiband rectenna for microwave applications. Comptes Rendus Physique. 2017;18(2):107-117

[69] Pham BL, Pham A. Triple bands antenna and high efficiency rectifier design for Rf energy harvesting at 900, 1900 and 2400 MHz. *IEEE MTT-S International Microwave Symposium Digest (MTT)*, USA. 2013

[70] Liu J, Zhang XY. Compact triple-band rectifier for ambient RF energy harvesting application. IEEE Access. 2018;6:19018-19024.

[71] Sarma SS, Chandravanshi S, Akhtar MJ. Triple band differential rectifier for RF energy harvesting applications. *Asia-Pacific Microwave Conference (APMC)*, New Delhi. 2016.

[72] Lopez-Yela A, Segovia-Vargas D. A triple-band bow-tie rectenna for RF energy harvesting without matching network. *IEEE Wireless Power Transfer Conference (WPTC)*, Taipei. 2017.

# **Appendix I:** Pin Diagram of IC7411, IC7404, IC 741

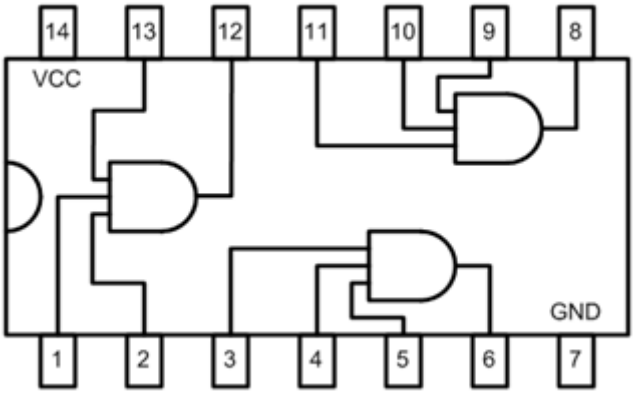


Fig: IC 7411(3 input AND gate)

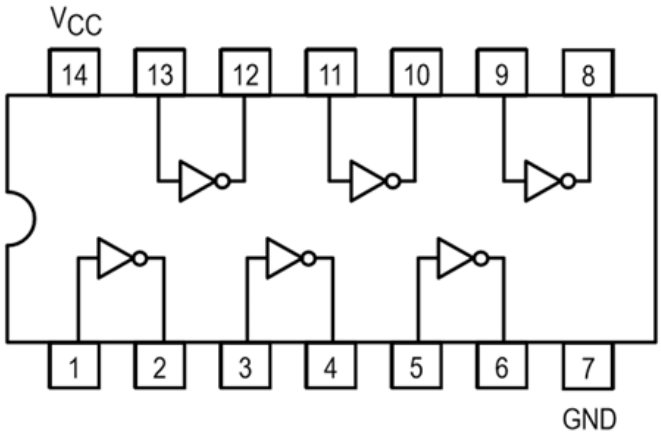


Fig: IC 7404(Hex inverter)

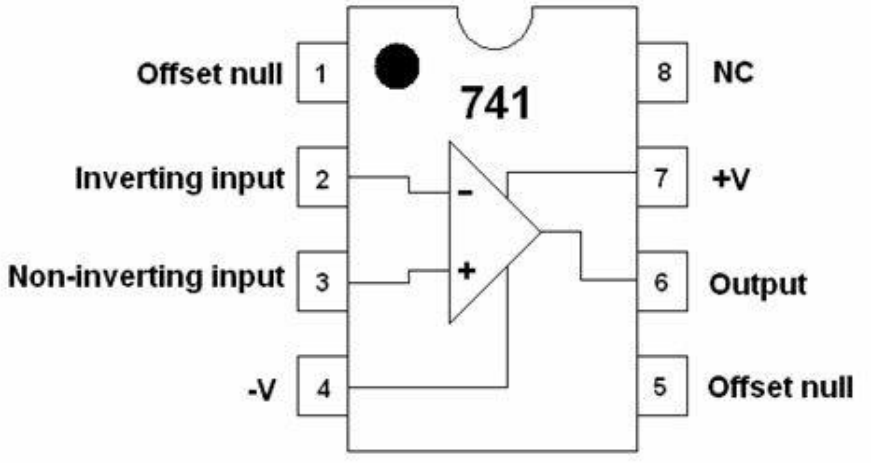


Fig: IC 741(Op-amp)

Gmail **Paramita Saha <saha.paramita90@gmail.com>**

# SPCOM 2022: Review Results [Paper #31]

**Microsoft CMT** <email@msr-cmt.org> Mon, Jun 6, 2022 at 10:44 PM
Reply-To: Sundeep Prabhakar Chepuri <spchepuri@iisc.ac.in>
To: Paramita Saha <saha.paramita90@gmail.com>

Dear Paramita Saha,

Paper ID: 31
Title: Smart Beam Steering with a Slot-Loaded Miniaturized Patch Antenna

Congratulations!

We are pleased to inform you that your manuscript has been accepted for presentation at IEEE SPCOM 2022 (https://ece.iisc.ac.in/~spcom/2022), which is to be held as a hybrid event in IISc, Bangalore in July 2022.

We received 366 submission, which were reviewed by technical program committee members who worked very hard to review the submissions. The review process resulted in a selection of 100 papers with an acceptance rate of 27.3%.

The reviewers' comments on your paper is available in your CMT profile.

The final camera-ready paper must be uploaded to the IEEE SPCOM 2022 paper submission site via CMT by June 17, 2022. To prepare the camera-ready paper, please carefully follow the instructions available on the webpage: https://ece.iisc.ac.in/~spcom/2022/camera_ready.html

Papers that do not conform to the official style may not be published.

More details about the author registration, video upload, technical program etc. will follow in due course.

Looking forward to welcoming you at IISc this July!

Yours sincerely,
Sundeep, Soma, Saif
IEEE SPCOM 2022, Technical Program Chairs


# Welcome to 2022 IEEE International Conference on Signal Processing and Communications (SPCOM)



## DAY 5: JULY 15 (Friday)

### Contributed Talks 13: Sparse Signal Processing

Venue: MP 20, Time: 9:30 - 11:00

Session Chair: Mrityunjoy Chakraborty, IIT Kharagpur

**Micro-Doppler Parameter Estimation Using Variational Mode Decomposition With Finite Rate of Innovation**
Shrikant Sharma (Indian Institute of Technology (IIT) Bombay); Adway Girish (IIT Bombay); Darin Jeff (Indian Institute of Technology (IIT) Bombay); Garweet Sresth (Indian Institute of Technology (IIT) Bombay); Sanket Bhalerao (Indian Institute of Technology (IIT) Bombay); C.H. Srinivas Rao (DRDO); P Radhakrishna (DRDO); Vikram M Gadre (IIT Bombay)

**On the Effective Sample Complexity for Exact Sparse Recovery from Sequential Linear Measurements**
Samrat Mukhopadhyay (IIT (ISM) Dhanbad)

**A Multi-Stage Constant False-Alarm Rate Detector for Millimeter Wave Radars**
Ganesan Thiagarajan (MMRFIC Tech. Pvt. Ltd.); Shilpa Hosur (PES University); Sanjeev Gurugopinath (PES University)

**Randomized Simultaneous Hard Thresholding Pursuit Algorithm for Multiple Measurement Vectors**
Ketan Atul Bapat (IIT Kharagpur); Mrityunjoy Chakraborty (IIT Kharagpur)

**Smart Device Localization Under α-KMS Fading Environment using Feedback Distance based Gradient Ascent**
Aditya Singh (Indian Institute of Technology Patna); Ankur Pandey; Dr Sudhir Kumar (IIT Patna)

## Plenary Talk 3: A light in digital darkness - Free space optics to connect the unconnected

Venue: Faculty Hall, Time: 11:30 - 12:30

Session Chair: KJ Vinoy, IISc Bangalore

**Title:** A light in digital darkness: Free space optics to connect the unconnected (Talk details (plenary.html#Alouini))

**Speaker:** Mohamed-Slim Alouini, Distinguished Professor, Electrical and Computer Engineering, KAUST

## Platinum Sponsor Keynote: What goes behind an Intelligent Camera? by Kiran Nanjunda Iyer, Samsung

Venue: Faculty Hall, Time: 12:30 - 13:00

Session Chair: KJ Vinoy, IISc Bangalore

## Contributed Talks 15: Terahertz Communications and RF Systems

Venue: MP 20, Time: 14:00 - 15:30

Session Chair: Priyanka Das, IIIT Bangalore

**Smart Beam Steering with a Slot-Loaded Miniaturized Patch Antenna**
Paramita Saha (Jadavpur University); Jagabandhu Das (SAMEER, Kolkata); PALANIANDAVAR VENKATESWARAN (Dept. of E.T.C.E., JADAVPUR UNIVERSITY)

**C-Band Iris Coupled Cavity Bandpass Filter**
Shashank Soi (DRDO); Sushil Singh (DRDO); Rajendra Singh (DRDO)

**A Wideband Bandpass Filter using U-shaped slots on SIW with two Notches at 8 GHz and 10 GHz**
Saragadam Siva Teja (National Institute of Technology Calicut); Tadikonda Jayanth (National Institute of Technology Calicut); Ramapuram Ajay Reddy (National Institute of Technology Calicut); Kanumetta Bhargava Ramanujam (National Institute of Technology Calicut); Shameer Keelaillam (National Institute of Technology calicut); Lalit Kumar (NIT Calicut)

**Intelligent Reflecting Surface Assisted Terahertz Communications**
Hemnta Kumar (IIT (BHU) Varanasi); Sanjeev Sharma (IIT BHU); Kuntal Deka (IIT Guwahati); Vimal Bhatia (IIT Indore)

## Contributed Talks 16: Image and Video Processing

# Smart Beam Steering with a Slot-Loaded Miniaturized Patch Antenna

Paramita Saha
Electronics & Telecommunication Engineering
Jadavpur University, Kolkata
Email: saha.paramita90@gmail.com

Jagabandhu Das
Department of Millimeter Integrated Chip Fabrication
SAMEER, Kolkata
Email: jagabandhu_das@rediffmail.com

Palaniandavar Venkateswaran
Electronics & Telecommunication Engineering
Jadavpur University, Kolkata
Email: pvwn@ieee.org

***Abstract*—In this paper, a smart beam steering technique is investigated with a miniaturized patch antenna at $2.45\ GHz$. The antenna is miniaturized with an asymmetrically placed slot on the patch that reduces the frequency of operation significantly. It radiates with $23\%$ area ($0.15\lambda X0.11\lambda$, $\lambda$ is the freespace wavelength at $2.45\ GHz$) of a conventional patch at the operating frequency with the same dielectric properties. A $1 \times 8$ antenna array is also designed with a power divider and phase shifter circuit to demonstrate a beam steering operation. With numerical investigation, a maximum of $22^0$ steering angle is observed in the azimuthal plane.**

***Index Terms*—smart beam steering, miniaturization with slot, patch antenna**

## I. Introduction

Smart beam steering technique is one of the most commonly used approaches adopted to improve the performance of a mobile and radar communication system. In the era of high-end technologies for commercial applications as well as for modern day electronic warfare, each mobile base station has to serve a large number of users simultaneously, without sacrificing the quality of communication. Moreover, the antenna mainbeam is to be steered towards a moving user for an uninterrupted communication with the base station.

Different beam steering techniques have been investigated over decades to steer the antenna main beam according to the requirement of the designer. A review of these techniques with corresponding pros and cons are discussed in [1]–[3]. In the phased array technique, the antenna main beam can be steered in the desired direction by controlling the input phase of individual antenna element of an array. Despite the requirement of additional phase shifter circuit, this approach provides an easy and accurate control over the steering angle. But it is preferable to miniature the circuit elements to design a compact system without sacrificing the system performances. Antenna being an indispensable component of any wireless transceiver system, provides a wide range of flexibility in its design [4]. Miniaturization of antennas is one of the most important topic for modern day antenna designers. Different techniques have been reported to make the antenna small [5] such as loading with dielectrics [6], slots [7] or even with metamaterials [8]. The slot based technique is one of the compact and easiest approaches in which no additional geometries are appended to the primary radiator. It introduces capacitive effect and elongates the current path to miniaturize the antenna element effectively.

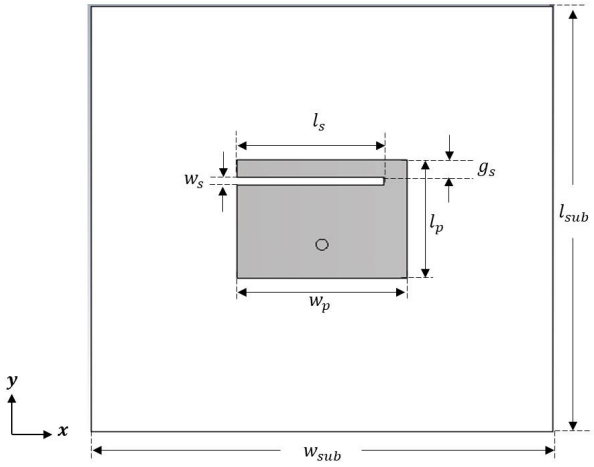


Fig. 1: Schematic of the proposed patch antenna (top view)

In this work, a smart beam steering technique is investigated with a slot based miniaturized patch antenna. The antenna design is optimized and an array is designed with a power divider phase shifter circuit to investigate the beam steering. A scheme of controlling the steering angle is also presented. The manuscript is arranged in the following sections: in Sec. II, miniaturization of patch antenna with a slot is investigated. In Sec. III, the antenna array and the power divider phase shifter circuit is presented with numerical results which is followed by the conclusion in Sec. IV.

## II. Design of Proposed Antenna

The reference antenna is a rectangular patch antenna designed to work at a higher frequency. Schematic of the antenna is similar to that in Fig. 1, but without the slot. The patch has a length of $l_p = 13.9\ mm$ and a width of $w_p = 18.4\ mm$ and is printed on a $FR-4$ ($\epsilon_r = 4.3$, $tan\delta = 0.025$) substrate of thickness $1.6\ mm$, with $l_{sub} = 50\ mm$ and $w_{sub} = 50\ mm$. The patch is excited with a coaxial line placed $3\ mm$ below the antenna centre.

The simulated $S_{11}$ of the reference antenna is shown in Fig. 2. The antenna resonates at around $5\ GHz$ ($4.84\ GHz$)

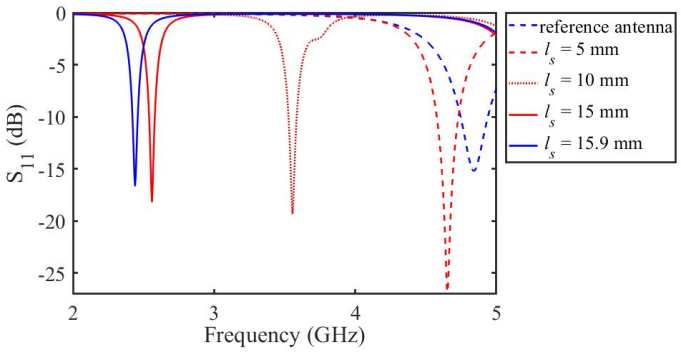


Fig. 2: Simulated $S_{11}$ of the reference antenna and the proposed antenna with varying slot length $l_s$

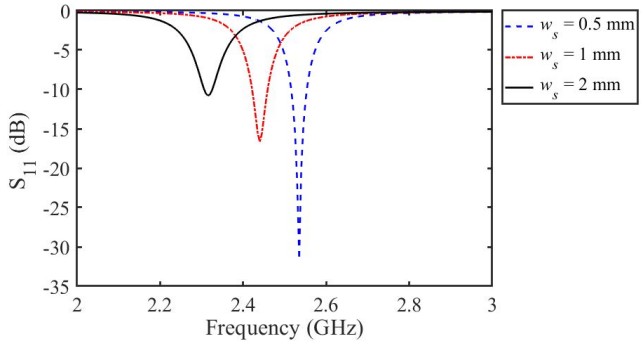


Fig. 3: Simulated $S_{11}$ with varying slot width $w_s$

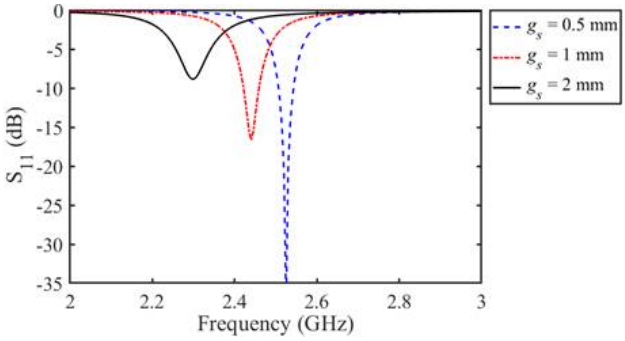


Fig. 4: Simulated $S_{11}$ with varying slot gap $g_s$

which is approximately double of the frequency interest of $2.45\ GHz$ (centre of the ISM band). The antenna dimensions are determined using [4]. To reduce the frequency of operation of this antenna, a horizontal slot is placed asymmetrically as shown in Fig. 1. The slot has a length of $l_s$ and width of $w_s$ maintains a gap of $g_s$ from the top edge. This slot significantly miniaturizes the antenna geometry as the radiation performances can be tuned by varying its dimensions, as is discussed in the following paragraphs.

### A. Effects of Slot Length ($l_s$)

Simulated responses by varying the slot length ($l_s$) are summarized in Fig. 2. Width of the slot ($w_s$) and its distance from the antenna top edge ($g_s$) are kept fixed at $1\ mm$. It can be observed that by increasing $l_s$, the resonant frequency can significantly be shifted at the low frequency band. For example, by varying the slot length from $5\ mm$ to $15\ mm$, the resonant frequency is shifted from $4.66\ GHz$ to $2.56\ GHz$, which is approximately half of that of the reference antenna. The antenna is resonated at $2.45\ GHz$ with $l_s = 15.9\ mm$. Since, a longer slot elongates the current path on antenna it reduces the resonant frequency significantly.

### B. Effects of Slot Width ($w_s$)

In this investigation, the slot width is varied by keeping $l_s = 15.9\ mm$ and $g_s = 1\ mm$. The simulated responses are summarized in Fig. 3. It is observed that, the resonant frequency shifts down by increasing the slot width. A higher $w_s$ increases the slot perimeter and hence the current path on antenna, thereby reducing the operating frequency of it. But, a wide slot affects the current distribution of the patch and affects the impedance at the feed point. This, degrades impedance matching of the antenna with an increase in $w_s$. The $S_{11} < -10\ dB$ is observed at $2.45\ GHz$ with $w_s = 1\ mm$.

### C. Effects of Slot Gap ($g_s$)

The simulated $S_{11}$ by varying slot gap ($g_s$) are summarized in Fig. 4. The slot length $l_s$ and width $w_s$ are fixed at $15.9\ mm$ and $1\ mm$, respectively. The resonant frequencies as well as impedance matching at those frequencies are affected by changing $g_s$, as in the previous investigation. By increasing $g_s$, the slot is placed closer to the feed that affects the impedance at this point and degrades the impedance matching at the operating frequency.

### D. Surface Current Distribution

To understand the miniaturization by the slot, the surface current distribution of the proposed structure at $2.45\ GHz$ is shown in Fig. 5. It can be observed that the current is maximum along the perimeter of the slot that explains the lower shift of the resonant frequency with an increase in the slot dimensions. As, much of the surface current surrounds the slot, its placement near the antenna feed significantly affects the impedance matching as is also observed in the previous investigations.

Considering these parametric studies, $l_s = 15.9\ mm$, $w_s = 1\ mm$ and $g_s = 1\ mm$ are dimension of the slot where the proposed patch antenna is resonated at $2.45\ GHz$. The proposed antenna is a miniaturized version of a conventional patch antenna working at the same frequency. The dimension of a conventional rectangular patch antenna considering the same dielectric property is approximately $29.2 \times 37.6\ mm^2$ for $2.45\ GHz$ [4]. The same resonant frequency is observed with the proposed patch of dimension $13.9 \times 18.4\ mm^2$ ($0.15\lambda \times 0.11\lambda$, $\lambda$ is the free space wavelength at $2.45\ GHz$) having $23\%$ area of the conventional patch. The maximum directivity is slightly sacrificed as the $5.53\ dBi$ of directivity is observed with the proposed patch instead of $6.32\ dBi$ with the conventional one. The reduction in directivity is due to

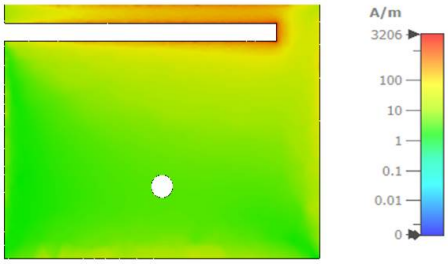


Fig. 5: Simulated surface current distribution of the proposed patch at 2.45 $GHz$

the increased beam width by the miniaturized aperture of the proposed antenna.

## III. Beam Steering with Proposed Antenna

The normalized array ($AF$) factor of an $N$-element linear array with uniform magnitude and distance is [4] -

$$AF = \frac{sin\frac{N}{2}\psi}{\frac{N}{2}\psi} \tag{1}$$

where, $\psi = kd\ cos\theta + \beta$, ($k$ : $2\pi/\lambda$, $d$ : distance between antennas, $\theta$ : angle of observation, $\beta$ : progressive phase between antennas).

The direction of maximum radiation ($\theta_m$) can be calculated with a $\theta$ value where the $AF$ is in the $sin(0)/0$ form -

$$\theta_m = cos^{-1}(\frac{\lambda\beta}{2\pi d}) \tag{2}$$

Therefore, by varying the input phases of the antennas progressively, the overall beam can be diverted at different angles ($\theta$) with the main lobe at $\theta_m$ direction.

In this section, the beam steering with the proposed antenna is investigated with an $1 \times 8$ array and the progressive phase shifts are implemented by an additional phase shift circuit. Schematic of the antenna array is shown in Fig. 6(a). The antennas are placed with a periodicity of 50 $mm$, which slightly less than $\lambda/2$ at the operating frequency of 2.45 $GHz$. A corporate feed configuration is used to feed all antennas with a single excitation. Phase shifter circuits are implemented by individually increasing the lengths of each feed line. The antenna and the circuit are printed on the top and bottom sides of a substrate separated by a common ground as shown in Fig. 6(b). An $FR-4$ substrate of thickness 1.6 $mm$ is placed above and below the ground plane. The feed ends are connected to the antenna using vias through holes in the ground plane.

### A. Power Divider and Phase Shifter Circuit

The power divider phase shifter circuit is shown in Fig. 6(a) (inset). The 50 $\Omega$ line (width $w_{50} = 3.1\ mm$) is divided into two 100 $\Omega$ (width $w_{100} = 0.72\ mm$) lines at each power division point. To match the input impedance of 50 $\Omega$, a quarter wave transmission line of impedance 70.7 $\Omega$ (length

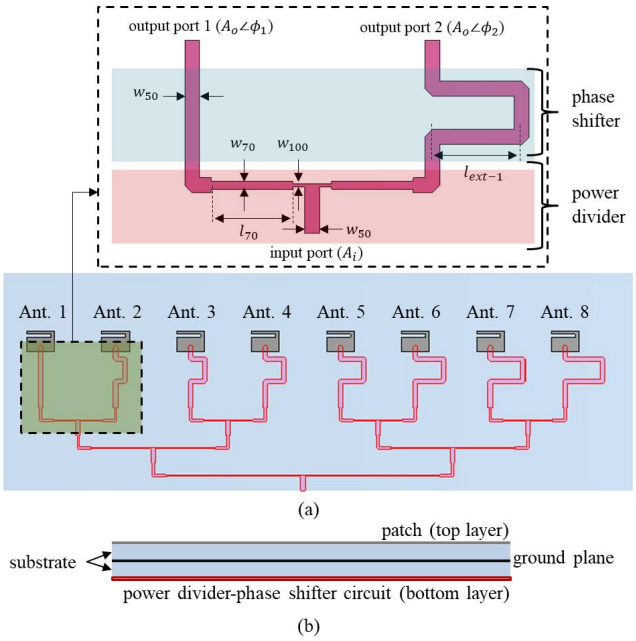


Fig. 6: $1 \times 8$ array of the proposed antenna showing (a) top view of antenna and power divider phase shifter circuit, highlighting the feed of port1 and port2 (inset), (b) side view showing different layers

$l_{70} = 17\ mm$ and width $w_{70} = 1.6\ mm$) is placed in between. Length of the 50$\Omega$ lines does not play any role in the design and hence are adjusted according to the placement of the antenna and the underlying circuits. A progressive phase shift from Ant. 1 to Ant. 8 is implemented by varying the length of the phase shifter section as indicated in Fig. 6(a) (inset). The first two feed lines to Ant. 1 and Ant. 2 are highlighted here. The feed line to Ant. 2 has an additional length of 2 $l_{ext-1}$ that produces an additional phase shift over the feed of Ant. 1. Therefore, both antennas are fed with signals of identical magnitude of $A_0$ (half of input power $A_i$) but with phases $\phi_1$ and $\phi_2$, respectively. The phase difference of $\angle\phi_2 - \angle\phi_1$ can be controlled by $l_{ext\ 1}$. Similar phase shift circuits are used for Ant. 3 to Ant. 8 with different additional lengths. A phase shift ($\phi_v$) vector is constructed with the added lengths from Ant. 1 to Ant. 8 as $\phi_v = [0,\ l_{ext-1},\ ,l_{ext-2}, ....., l_{ext-7}]$.

### B. Demonstration of Beam Steering

As the phase shifts are implemented with additional lengths to the feed paths, the antenna beam can only be steered at a certain direction for a fixed $\phi_v$. To vary the steering angle, $\phi_v$ is varied by multiplying it with a constant $mul$ that would change the relative phase differences among the antennas, thereby steering the beam at different angles. The average phase shift in the antenna excitation ($\phi_{avg}^{exi}$) for different values of $mul$ are summarized in the Table I. It can be observed that the input phases can be suitably varied by changing the $mul$.

The normalized radiation patterns on $\phi = 0^0$ plane ($zx$ plane) are plotted for different $mul$ in Fig. 7. The direction of maximum radiation ($\theta_m$) is also summarized in Table I. It can

TABLE I: Variation in $\phi_{avg}^{exi}$ and $\theta_m$ with $mul$

| $mul$ | 0.6 | 1 | 1.8 | 2.2 |
|---|---|---|---|---|
| $\phi_{avg}^{ext}$ | $13.96^0$ | $24.9^0$ | $49.64^0$ | 60.8 |
| $\theta_m$ | $4^0$ | $12^0$ | $19^0$ | $22^0$ |

be observed that the main beam is guided in boresight ($\theta = 0^0$) without any phase shifter when all antennas are excited with same phase. The overall array has a 3 $dB$ beamwidth of approximately $16^0$. Initially the following $\phi_v$ is considered to be $\phi_v = [0, 4.75, 7.25, 9.5, 11.9, 14.4, 16.8, 19.2]$ (in $mm$, $mul = 1$), for a squint angle of approximately $12^0$. For $mul = 0.6$, the steer angle of $4^0$ is observed due to the reduced phase shifts among the antennas. To squint the beam at a higher angle, $mul = 1.8$ and 2.2 are investigated and the patterns are plotted in the same figure. The beam is guided at approximately $19^0$ and $22^0$ away from boresight in these cases. Therefore, the $mul$ can be suitably varied to steer the antenna main beam at different angular locations. Further increase in $mul$ can result in an overlapping between the adjacent circuits, hence are avoided in this investigation. Intuitively it is understood that, the beam can be steered at the $-\theta_m$ direction by connecting the phase shifter circuit in the opposite order, $i.e.$, by putting a regressive shift from Ant. 1 to Ant. 8. An electronic phase shift can be used by replacing the current phase shifter section to facilitate a seamless steering of the antenna mainbeam over a wide angular region.

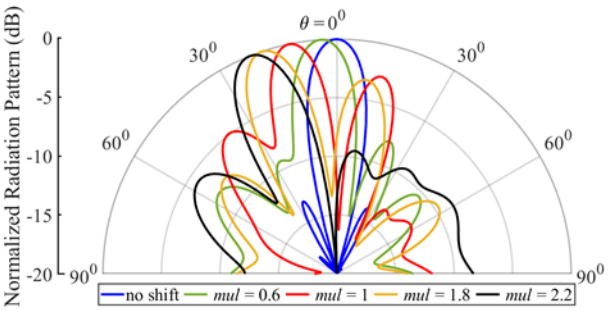


Fig. 7: Steering of antenna main beam on $\phi = 0^0$ plane by varying $mul$

## IV. Conclusion

A smart beam steering technique is investigated for the ISM band (2.45 $GHz$) using a slot based miniaturized patch antenna. The slot is asymmetrically placed on a rectangular patch to resonate it at a lower frequency. The dimensions and placement of it is varied to observe the effects on the overall antenna performance with numerical outputs. The surface current is also plotted to explain the working of the slot with more physical insight. The proposed antenna ($0.15\lambda \times 0.11\lambda$) is radiated at the operating frequency with 23% area of that of a conventional rectangular patch antenna at this frequency. Hence, the proposed design is compact and cost effective compared to a conventional patch antenna. To investigate the beam steering, an $1 \times 8$ array is designed and the input phases of individual antennas are controlled. The power divider phase shifter circuit is also designed to excite the antennas with a progressive phase shift. A two layered substrate is used to place the antenna and the circuit on the opposite sides of it. A maximum of $22^0$ tilt is observed with the array by varying the input phases suitably. A possibility of using an electronic phase shift circuit for a seamless steering is also discussed. The proposed circuit can be used in conjunction with a tracking system to design a complete transceiver chain for a track based smart beam steering network. Further investigations can be carried out for higher steering angles along with its experimental validation with a fabricated prototype which is left as a future work.

## References


[1] A. Singh, A. Kumar, A. Ranjan, A. Kumar and A. Kumar, "Beam steering in antenna," *2017 International Conference on Innovations in Information, Embedded and Communication Systems (ICIIECS)*, 2017, pp. 1-4.

[2] T. Kushwaha, D. K. Singh, "A Review on Beam Steering Techniques in Reconfigurable Microstrip Patch Antennas," *International Journal of Advanced Research in Computer Engineering & Technology (IJARCET)*, Vol. 6, Issue 9, Sep. 2017.

[3] I. E. Uchendu, J. R. Kelly, R. Mittra and Y. Gao, "Hybrid Parasitic Linear Array Antenna for Fine Beamsteering Applications," *IEEE Access*, vol. 9, pp. 84899-84909, 2021.

[4] C. A. Balanis,"Antenna Theory: Analysis and Design," *Wiley-India*, 2nd ed., 2009.

[5] A. A. Rakholiya, N. V. Langhnoja, "A review on miniaturization techniques for microstrip patch antenna," *International Journal of Advance Research and Innovative Ideas in Education (IJARIIE)*, vol. 3, issue 2, 2017.

[6] D. Schaubert and K. Yngvesson, "Experimental study of a microstrip array on high permittivity substrate," *IEEE Transactions on Antennas and Propagation*, vol. 34, no. 1, pp. 92-97, January 1986.

[7] S. I. Hussain Shah, S. Bashir and A. Altaf, "Miniaturization of microstrip patch antenna by using various shaped slots for wireless communication systems," *2014 XIXth International Seminar/Workshop on Direct and Inverse Problems of Electromagnetic and Acoustic Wave Theory (DIPED)*, 2014, pp. 92-95.

[8] T. K. Upadhyaya, V. V. Dwivedi, S. P. Kosta and Y. P. Kosta, "Miniaturization of Tri Band Patch Antenna Using Metamaterials," *2012 Fourth International Conference on Computational Intelligence and Communication Networks*, 2012, pp. 45-48